

Towards Efficient LLM Grounding for Embodied Multi-Agent Collaboration

Yang Zhang^{1*†}, Shixin Yang^{2*}, Chenjia Bai^{3,5‡},
Fei Wu⁴, Xiu Li¹, Zhen Wang², Xuelong Li³

¹Tsinghua University, ²Northwestern Polytechnical University,
³Institute of Artificial Intelligence (TeleAI), China Telecom, ⁴Zhejiang University,
⁵Shenzhen Research Institute of Northwestern Polytechnical University

Abstract

Grounding the reasoning ability of large language models (LLMs) for embodied tasks is challenging due to the complexity of the physical world. Especially, LLM planning for multi-agent collaboration requires communication of agents or credit assignment as the feedback to re-adjust the proposed plans and achieve effective coordination. However, existing methods that overly rely on physical verification or self-reflection suffer from excessive and inefficient querying of LLMs. In this paper, we propose a novel framework for multi-agent collaboration that introduces Reinforced Advantage feedback (ReAd) for efficient self-refinement of plans. Specifically, we perform critic regression to learn a sequential advantage function from LLM-planned data, and then treat the LLM planner as an optimizer to generate actions that maximize the advantage function. It endows the LLM with the foresight to discern whether the action contributes to accomplishing the final task. We provide theoretical analysis by extending advantage-weighted regression in reinforcement learning to multi-agent systems. Experiments on Overcooked-AI and a difficult variant of RoCoBench show that ReAd surpasses baselines in success rate, and also significantly decreases the interaction steps of agents and query rounds of LLMs, demonstrating its high efficiency for grounding LLMs. More results are given at <https://embodied-read.github.io/>.

1 Introduction

Benefiting from large-scale text corpora from the web (Devlin et al., 2019; Radford et al., 2019; Brown et al., 2020; Raffel et al., 2020), LLMs absorb vast world knowledge for decision-making. Recent research (Firoozi et al., 2023; Yao et al., 2023b; Song et al., 2023a) has shown that LLMs

can perform planning and solve embodied tasks using zero-shot or few-shot example prompting, based on a closed-loop framework to refine LLM outputs through feedback. Existing methods that design a closed-loop framework can be roughly divided into two lines. Specifically, one line of research adopts *self-reflection* by performing self-evaluation by LLMs to improve the plan generation of LLM planner (Shinn et al., 2023; Yao et al., 2023b; Hao et al., 2023; Liu et al., 2023b); and the other works perform *physical verification* by using feedback from the external environment to dynamically replan depending on unexpected feedback (Huang et al., 2022b; Song et al., 2023a). Despite these efforts, the feedback is often sparse or heuristic, and a more principled feedback mechanism for LLM-based embodied task planning is still lacking.

The challenge becomes even more pronounced in embodied multi-agent settings, where LLM-based agents must communicate and negotiate to cooperate effectively. Both self-reflection and physical verification struggle to evaluate the impact of individual actions on team outcomes, leading to inefficiencies such as excessive LLM queries or frequent environmental interactions. For instance, RoCo (Mandi et al., 2023) integrates physical verification to refine LLM-generated actions in multi-agent scenarios but suffers from poor efficiency due to excessive interactions. As shown in Figure 1, RoCo requires excessive interaction to obtain physical feedback and queries to LLMs to get feasible joint-action plans, resulting in the failure. In contrast, various methods in Multi-Agent Reinforcement Learning (MARL) (Zhang et al., 2021) have developed value or advantage decomposition theories (Rashid et al., 2020; Kuba et al., 2022a,b), which evaluate individual contributions on a team outcome and improve the coordination. Inspired by these principles, we ask "*How can we enhance the reasoning efficiency of LLMs for embodied multi-agent collaboration with theoretical supports of*

*Equal Contributions.

†Work done during the internship at TeleAI.

‡Correspondence to: <baicj@chinatelecom.cn>.

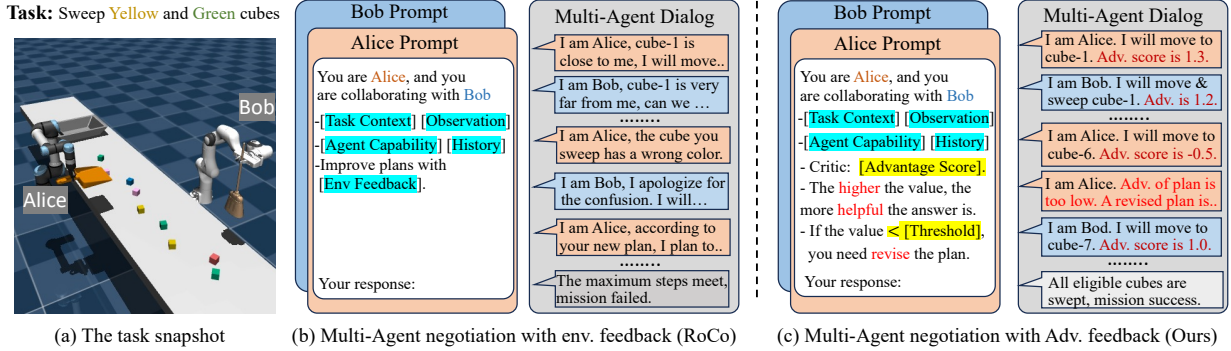


Figure 1: An illustration of the negotiation process of RoCo and our method. RoCo interacts with the environment for each plan and takes the environment’s feedback as prompts. In contrast, our method takes the advantage function (Adv.) evaluated by a critic as feedback, and revises the plan if the advantage value is lower than the threshold, which significantly reduces the interaction rounds to the environment.

MARL?”. Our objective is to develop an efficient feedback and refinement algorithm by utilizing multi-agent advantage functions, for multi-agent planning assisted by LLMs.

To this end, we propose **Reinforced Advantage (ReAd)**, a closed-loop feedback mechanism for LLMs in embodied multi-agent collaboration. ReAd offers two plan refinement schemes: (i) Joint Plan Refinement (named **ReAd-J**) evaluates the advantage of joint actions, which requires LLMs to generate the joint plans of all agents at once; (ii) Sequential Individual Plan Refinement (named **ReAd-S**) evaluates the local advantages of each agent’s action based on multi-agent advantage decomposition (Kuba et al., 2022a), which allows LLMs to generate actions for each agent sequentially. Both advantages are estimated by a critic network that regresses LLM-planned data. Based on the critic, an LLM planner is used as an optimizer by prompting to generate actions that maximize the advantage value. Otherwise, the LLM planner is required to re-plan if the advantage value is small. We provide a theoretical motivation for such a process by extending advantage-weighted regression (Peng et al., 2019) to multi-agent settings. In experiments, we extend RoCoBench (Mandi et al., 2023) to a difficult variant, which we term *DV-RoCoBench*. Results on *DV-RoCoBench* and our adapted *Overcooked-AI* show that ReAd significantly decreases the interaction and query rounds, and also surpasses baselines in success rate, highlighting its effectiveness for grounding LLMs in multi-agent collaboration tasks.

2 Preliminaries

We consider a Markov game, which is defined by a tuple $\langle \mathcal{N}, \mathcal{S}, \mathcal{A}, P, r, \gamma \rangle$, in which \mathcal{N} de-

notes the set of agents, \mathcal{S} denotes state space, $\mathcal{A} = \prod_{i=1}^n \mathcal{A}^i$ denotes the product of finite action spaces of all agents (i.e., joint action space), $P : \mathcal{S} \times \mathcal{A} \times \mathcal{S} \rightarrow [0, 1]$ denotes the transition probability function, $r : \mathcal{S} \times \mathcal{A} \rightarrow \mathbb{R}$ denotes the reward function, and $\gamma \in [0, 1)$ denotes the discount factor. In the Markov game, every agent at time step $t \in \mathbb{N}$ observes the state of environment $s_t \in \mathcal{S}$ and takes an action $a_t^i \in \mathcal{A}^i$ from its corresponding policy $\pi^i(\cdot|s_t)$, which together with other agents’ actions forms a joint action $\mathbf{a}_t = (a_t^1, a_t^2, \dots, a_t^n) \in \mathcal{A}$ drawn from the joint policy $\pi(\cdot|s_t) = \prod_{i=1}^n \pi^i(\cdot|s_t)$. Then agents receive a shared reward $r_t = r(s_t, \mathbf{a}_t)$ and observe a new state s_{t+1} with probability $P(s_{t+1}|s_t, \mathbf{a}_t)$. With the joint policy π and the transition probability function P , the state value function is defined as $V_\pi(s) \triangleq \mathbb{E}_{s_{1:\infty} \sim P, \mathbf{a}_{0:\infty} \sim \pi} [\sum_{i=0}^{\infty} \gamma^i r_i | s_0 = s]$. And the state-action value function is defined as $Q_\pi(s, \mathbf{a}) \triangleq \mathbb{E}_{s_{1:\infty} \sim P, \mathbf{a}_{1:\infty} \sim \pi} [\sum_{i=0}^{\infty} \gamma^i r_i | s_0 = s, \mathbf{a}_0 = \mathbf{a}]$. We aim at finding a joint policy to maximize the expected return $J(\pi) \triangleq \mathbb{E}_{s_{0:\infty} \sim P, \mathbf{a}_{0:\infty} \sim \pi} [\sum_{t=0}^{\infty} \gamma^t r_t]$. In the following, we consider the LLM planner as a special RL policy, which can be evaluated by a value function.

3 Methodology

We first give definitions and learning algorithms for two kinds of advantage functions in §3.1. Then, we provide theoretical motivation for efficient LLM grounding by extending advantage-weighted regression to multi-agent settings in §3.2. Finally, we describe how to derive Reinforced Advantage (ReAd) feedback from the motivation and use an LLM planner as an optimizer and refine the plan in §3.3.

3.1 Learning of Advantage Functions

We first introduce the estimation of *joint* advantage function. Then the *local* advantage is obtained via advantage decomposition by following theories from MARL.

Joint Advantage Function. Based on joint value functions $Q_\pi(s, \mathbf{a})$ and $V_\pi(s)$, we define the *joint* advantage function as

$$A_\pi(s, \mathbf{a}) \triangleq Q_\pi(s, \mathbf{a}) - V_\pi(s),$$

which evaluates the advantage value of joint actions $\mathbf{a}_t = (a_t^1, a_t^2, \dots, a_t^n)$ from all agents. $A_\pi(s, \mathbf{a})$ will be used for *ReAd-J* to evaluate the joint planning of all agents as feedback. Here, we assume the option of taking no actions is available to each agent, which is reasonable and common in embodied tasks. With this special action that we term *WAIT*, we can estimate the joint advantage using only $Q_\pi(s, \mathbf{a})$.

When taking *WAIT* action $a = w$, the agent will keep dormant at the current time step. The joint *WAIT* action is denoted as $\mathbf{w} = (w, w, \dots, w)$. Choosing \mathbf{w} at the current state s signifies all agents take no actions, then the next state $s' = s$ and the agents receive shared reward $r(s, \mathbf{w}) = 0$ since \mathbf{w} bring no changes to the environment. Then we can hold the following relationship. The detailed derivation is provided in §A.1.

$$A_\pi(s, \mathbf{a}) = Q_\pi(s, \mathbf{a}) - \frac{1}{\gamma} Q_\pi(s, \mathbf{w}). \quad (1)$$

Local Advantage Function. In cooperative multi-agent settings, we can further consider the contribution to performance in different subsets of agents' views. We adopt the standard definition in MARL to measure the local advantages.

Definition 1. (Kuba et al., 2022a) Let $i_{1:m}$ denote an ordered subset $\{i_1, \dots, i_m\}$ of \mathcal{N} , and let $-i_{1:m}$ refer to its complement. We mark i_k when we refer to the k^{th} agent in the ordered subset. Correspondingly, the multi-agent local state-action value function is defined as

$$Q_\pi^{i_{1:m}}(s, \mathbf{a}^{i_{1:m}}) \triangleq \mathbb{E}_{\mathbf{a}^{-i_{1:m}} \sim \pi^{-i_{1:m}}} [Q_\pi(s, \mathbf{a}^{i_{1:m}}, \mathbf{a}^{-i_{1:m}})] \quad A_\pi(s, \mathbf{a}) = \sum_{k=1}^n A_\pi^{i_k}(s, \mathbf{a}^{i_{1:k-1}}, a^k), \quad (4)$$

and for disjoint sets $j_{1:k}$ and $i_{1:m}$, the multi-agent local advantage function is

$$A_\pi^{i_{1:m}}(s, \mathbf{a}^{j_{1:k}}, \mathbf{a}^{i_{1:m}}) \triangleq Q_\pi^{j_{1:k}, i_{1:m}}(s, \mathbf{a}^{j_{1:k}}, \mathbf{a}^{i_{1:m}}) - Q_\pi^{j_{1:k}}(s, \mathbf{a}^{j_{1:k}}) \quad (3)$$

Monte Carlo Estimation. Both Eqs. (1) and (3) can be estimated via the local value function $Q_\pi^{i_{1:m}}(s, \mathbf{a}^{i_{1:m}})$ with arbitrary action subset $\mathbf{a}^{i_{1:m}}$. More precisely, the local advantages can be estimated by changing $\mathbf{a}^{i_{1:m}}$ to disjoint action sets or subsets, and the joint advantages can be obtained by changing $\mathbf{a}^{i_{1:m}}$ to $\mathbf{a}^{1:n}$ that contains the joint actions or the joint *WAIT* action. In the following, we denote the underlying policy of the LLM planner as $\mu = \pi_{\text{llm}}(\mathbf{a}|s)$. To estimate $Q_\mu^{i_{1:m}}$, we collect a dataset \mathcal{D} by following the behavior policy μ , and further augment it with enhanced trajectories to overcome the out-of-distribution (OOD) problem of action estimation (Levine et al., 2020). Then we estimate $Q_\mu^{i_{1:m}}(s, \mathbf{a}^{i_{1:m}})$ via Monte Carlo estimation by following $\mathcal{R}_{s, \mathbf{a}^{i_{1:m}}} = \sum_{\mathbf{a}^{-i_{1:m}} \in \mathcal{D}} \sum_{t=0}^T \gamma^t r_t$, where the complement sets is sampled from the dataset. Then the value function is learned by a regression loss as

$$\mathbb{E}_{s, \mathbf{a}^{i_{1:m}} \sim \mathcal{D}} [\|\mathcal{R}_{s, \mathbf{a}^{i_{1:m}}} - Q_\mu^{i_{1:m}}\|^2].$$

We refer to Alg. 1 in §C for the details. The setting of reward r_t depends on the specific task, e.g., for sweeping cubes in Figure 1, $r_t = 1$ if a correct cube is swept and $r_t = 0$ otherwise. The details of data collection are given in §E.6.

Advantage Decomposition. Based on Eq. (2), we can express the state value function $V_\pi(s)$ in a new form. Given the whole set of agents $\mathcal{N} = \{1, \dots, n\}$,

$$V_\pi(s) = \mathbb{E}_{\mathbf{a}^{1:n} \sim \pi^{1:n}} [Q_\pi(s, \mathbf{a}^{1:n})].$$

Based on Definition 1, we can introduce a pivotal lemma, which reveals that joint advantage function can be decomposed into the summation of local advantages of each agent.

Lemma 1. (Multi-Agent Advantage Decomposition). In any cooperative Markov games, given a joint policy π and the whole set of agents $\mathcal{N} = \{1, \dots, n\}$, for any state s , and any ordered set $i_{1:n}$ of all agents, we have

where $\mathbf{a} = (a^1, a^2, \dots, a^n)$.

The proof follows Kuba et al. (2022a) and is given in §A.2. Lemma 1 will be used for derivation in §3.2.

3.2 Theoretical Motivation for Grounding LLM

In this section, we give a theoretical motivation that closely resembles advantage-weighted regression (Peng et al., 2019) in single-agent RL, while we extend it for multi-agents via advantage decomposition in Lemma 1. To achieve efficient LLM grounding, i.e., to obtain a superior policy to the LLM planner, one option is adopting LLM as a basic policy and searching for a stronger policy than it. Therefore, we derive our objective as an approximate optimization of a constrained policy search problem. Specifically, we denote the policy of LLM planners as $\mu = \pi_{\text{llm}}(\mathbf{a}|s)$, and our goal is to find a policy π that maximizes the expected improvement $\eta(\pi) = J(\pi) - J(\mu)$ over the basic policy μ . Following the performance difference lemma (Kakade and Langford, 2002; Schulman et al., 2015), we show the expected improvement $\eta(\pi)$ can be expressed in terms of the advantage over $\mu(\mathbf{a}|s)$, as

$$\eta(\pi) = \mathbb{E}_{s \sim \rho_{\pi}(s), \mathbf{a} \sim \pi(\mathbf{a}|s)} [A_{\mu}(s, \mathbf{a})], \quad (5)$$

where $\rho_{\pi}(s) = \sum_{i=0}^{\infty} \gamma^i P(s_i = s)$ is the (unnormalized) discounted visitation frequencies over policy π . Since the objective in Eq. (5) is difficult to optimize due to the dependency on $\rho_{\pi}(s)$ and π , we introduce a surrogate objective $\hat{\eta}(\pi)$ to approximate $\eta(\pi)$, instructed by Schulman et al. (2015), as

$$\hat{\eta}(\pi) = \mathbb{E}_{s \sim \rho_{\mu}(s), \mathbf{a} \sim \pi(\mathbf{a}|s)} [A_{\mu}(s, \mathbf{a})], \quad (6)$$

with the constraint that the new policy π is close enough to the basic policy μ^1 , i.e., the KL divergence between π and μ $D_{\text{KL}}(\pi(\cdot|s) \parallel \mu(\cdot|s)) \leq \epsilon$.

Optimal Joint Policy. The optimal policy π^* for the above surrogate constrained optimization problem is expressed by,

$$\pi^*(\mathbf{a}|s) = \frac{1}{Z(s)} \mu(\mathbf{a}|s) \exp\left(\frac{1}{\beta} A_{\mu}(s, \mathbf{a})\right), \quad (7)$$

where $Z(s)$ is the partition function.

Optimal Individual Policy. Following advantage decomposition in Lemma 1, we can decompose the optimal joint policy $\pi^*(\mathbf{a}|s)$ to optimal individual policies by assuming the agents choose

actions sequentially in the order of $1, 2, \dots, n$, as

$$\begin{aligned} \pi^*(a^i|s, \mathbf{a}^{1:i-1}) \\ = \frac{\mu^i(a^i|s, \mathbf{a}^{1:i-1})}{Z^i(s)} \exp\left(\frac{1}{\beta} A_{\mu}^i(s, \mathbf{a}^{1:i-1}, a^i)\right) \end{aligned} \quad (8)$$

where $Z^i(s)$ is the partition function. We refer to §A.3 for a detailed derivation of Eqs. (7) and (8).

By maximizing the expected policy improvement $\eta(\pi) = J(\pi) - J(\mu)$, we obtain stronger joint and individual policies (i.e., $\pi^*(\mathbf{a}|s)$ and $\pi^*(a^i|s, \mathbf{a}^{1:i-1})$) over the basic policy $\mu = \pi_{\text{llm}}$. The key insight behind the policy improvement is to re-weight the LLM policy with exponential weights defined in terms of advantages. The advantage function is estimated by local value function $Q_{\mu}^{i:u}(s, \mathbf{a}^{1:u})$, where we calculate it via Monte-Carlo estimation from a collected dataset \mathcal{D} , as we discussed in §3.1.

3.3 Prompting by Reinforced Advantage Feedback

Upon the basic policy $\mu = \pi_{\text{llm}}$, the advantage-weighted solution in Eq. (8) offers a crucial intuition that (i) by increasing the probability of $\mu^i(a_{\text{pos}}^i|s, \mathbf{a}^{1:i-1})$ for those actions a_{pos}^i with positive advantages, i.e., $A_{\mu}^i(s, \mathbf{a}^{1:i-1}, a_{\text{pos}}^i) > 0$, and (ii) decreasing the probability of $\mu^i(a_{\text{neg}}^i|s, \mathbf{a}^{1:i-1})$ for those actions a_{neg}^i with negative advantages, i.e., $A_{\mu}^i(s, \mathbf{a}^{1:i-1}, a_{\text{neg}}^i) < 0$, we can ensure an expected performance improvement over $J(\mu)$. Therefore, Eq. (8) can be equivalently viewed as behavior cloning (BC) on the *exponential weighting* dataset $\bar{\mathcal{D}}$ where the better actions are given by higher weights $e^{A_{\mu}^i(s, \mathbf{a}^{1:i-1}, a^i)/\beta}$. When β is sufficiently small, it becomes BC on a dataset processed by *binary filtering* $\mathbb{1}[A_{\mu}^i(s, \mathbf{a}^{1:i-1}, a^i) > 0]$ where $\mathbb{1}$ is the indicator function. This provides an ideal alternative for improving μ without access to the exact probability of the sampled action $a^i \sim \mu^i(\cdot|s, \mathbf{a}^{1:i-1})$, there being convenient for grounding close-source LLMs. We provide theoretical proof for the monotonic improvement with the *binary filtering* in §A.4.

Inspired by the *binary filtering*, we develop a novel feedback mechanism, wherein the main idea is to convert the filter $\mathbb{1}[A_{\mu}^i(s, \mathbf{a}^{1:i-1}, a^i) > \epsilon \geq 0]$ into the feedback of LLM-proposed plans with their corresponding scores $A_{\mu}^i(s, \mathbf{a}^{1:i-1}, a^i)$ for refining the plans. Based on different types of advantages, we design two algorithms for plan refine-

¹We refer to Schulman et al. (2015) for details.

ment: *ReAd-S* and *ReAd-J*. The process of prompting and refinement is depicted in Figure 2. Algorithmic details of *ReAd-S* and *ReAd-J* are given in §C.

Prompting and Refinement for *ReAd-S*. For each time step, we initialize an empty action-set $\mathbf{a}_t = \{\}$ and follow the order of $[1, \dots, n]$ for agents in planning. For planning action a_t^i of agent i at state s_t , the process of *ReAd-S* contains two parts. (i) **Prompting as Optimizing.** An LLM planner is given the history of advantages of previous state-action pairs, i.e., $\mathcal{H} = \{(s, (\mathbf{a}^{1:i-1}, a^i), A_\mu^i(s, \mathbf{a}^{1:i-1}, a^i))\}$, and is prompted to *choose an action with the highest advantage* for agent i , which recovers the principle of advantage-weighted regression. Leveraging the in-context learning ability, we hope the LLM planner can induce the advantage values of available actions implicitly and choose the action a_t^i with the highest advantage. This process is inspired by recent work for LLM as optimizer (Yang et al., 2023), where the agent is prompted to give a plan that optimizes a score function. (ii) **Feedback for Refinement.** Nevertheless, the implicit advantage maximizing can be hard since the number of available actions can be large. Thus, we introduce a refinement process to allow the LLM to refine the policy if an unsatisfactory action is generated. We use the pre-trained critic network $Q_\theta^{i:u}(s, \mathbf{a}^{i:u})$ with parameter θ to estimate the advantage score of a generated action, as

$$\begin{aligned} \mathbb{S}_{\text{ReAd-S}}(a_t^i) &= A_\theta^i(s_t, \mathbf{a}_t^{1:i-1}, a_t^i) \\ &= Q_\theta^{1:i}(s_t, \mathbf{a}_t^{1:i-1}, a_t^i) - Q_\theta^{1:i-1}(s_t, \mathbf{a}_t^{1:i-1}). \end{aligned}$$

Given a threshold $\epsilon \geq 0$, if the score function is less than the threshold (i.e., $\mathbb{S}_{\text{ReAd-S}}(a_t^i) < \epsilon$), we add this failed action to the history \mathcal{H} and prompt the agent to re-plan. Such a refinement guarantees embodied agents always take the actions with $A_\theta^i(s_t, \mathbf{a}_t^{1:i-1}, a_t^i) > \epsilon$, further ensuring monotonic improvements over π_{llm} . It significantly decreases the interaction rounds of agents since the action a_t^i has been evaluated and refined via advantage feedback before execution. In contrast, previous methods like RoCo need to interact with the environment to get physical feedback regardless of the quality of the generated actions. The refined action is added into the action-set $\mathbf{a}_t \leftarrow \mathbf{a}_t \cup \{a_t^i\}$ and we then perform sequential decision for agent $i + 1$.

Prompting and Refinement for *ReAd-J*. The planning process of the LLM planner for *ReAd-J* is

similar to that of *ReAd-S*. The main difference is the LLM planner for *ReAd-J* is required to give a joint action \mathbf{a}_t for all agents at once. Meanwhile, we use the joint advantage function for history prompting with $\mathcal{H} = \{(s, \mathbf{a}_t, A_\mu(s_t, \mathbf{a}_t))\}$ rather than considering the local advantages. The score function is

$$\begin{aligned} \mathbb{S}_{\text{ReAd-J}}(\mathbf{a}_t) &= A_\theta(s_t, \mathbf{a}_t) \\ &= Q_\theta(s_t, \mathbf{a}_t) - 1/\gamma Q_\theta(s_t, \mathbf{w}) \end{aligned}$$

based on Eq. (7). The joint plan \mathbf{a}_t is refined if it is less than a threshold (i.e., $\mathbb{S}_{\text{ReAd-J}}(\mathbf{a}_t) < \epsilon$).

4 Related Works

We discuss with the most relevant literature here and provide more in-depth discussions in §B.

Grounding LLM with RL. RL with Human Feedback (RLHF) has been used to align LLM with human preference through parameter tuning (Dai et al., 2023; Fernandes et al., 2023; Song et al., 2023b). In contrast, our work focuses on grounding closed-source LLM with RL via few-shot prompting and closed-loop feedback (Zeng et al., 2023; Wu et al., 2023; Huang et al., 2022a; Lin et al., 2023b). Previous works tried to integrate RL into LLM planning under the framework tree search (Browne et al., 2012). For example, Fafa (Liu et al., 2023b) and TS-LLM (Feng et al., 2023) learn an environment model and value function to plan the subroutine in MCTS. REX (Murthy et al., 2023) proposes to balance exploration and exploitation in LLM-based MCTS. Other works like SayCan (Ahn et al., 2022) and Text2Motion (Lin et al., 2023d) adopt a model-free manner by learning value functions to connect LLM knowledge to physical environments. SwiftSage (Lin et al., 2023a) performs imitation learning for rapid thinking and LLM for methodical training. Remember (Zhang et al., 2023b) learns value functions for LLM to predict Q -value via exemplars in prompts and select actions based on Q -values. Unlike the Remember framework, which retrieves similar states from a buffer, we evaluate the advantage function of planned actions via a neural network and follow advantage-weighted regression in prompting. We employ the advantage function in a multi-agent setting, while previous methods focus on single-agent planning. Previous LLM-based multi-agent works mostly manually designed communication, reflection, and reasoning modules (Zhang et al., 2023a,c; Kannan et al., 2023; Chen et al., 2023). CAMEL

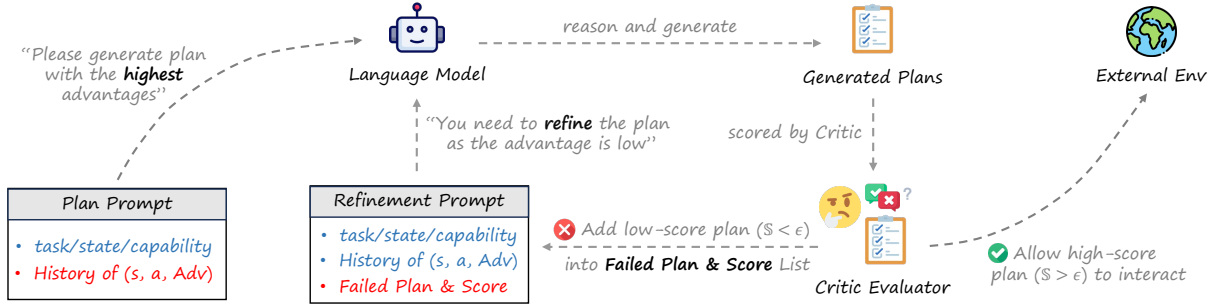


Figure 2: An overview of prompting and refinement. For each timestep t , the LLM planner is given the history, which contains states, actions, and advantages, and is prompted to generate a plan with the highest advantage. The pre-trained critic is used to evaluate the score of the generated action $\mathbb{S}_{\text{ReAd}}(a_t^i)$. If $\mathbb{S}_{\text{ReAd}}(a_t^i) < \epsilon$, the failed plan is used as a prompt, and the LLM planner is asked to refine the policy until the $\mathbb{S}_{\text{ReAd}}(a_t^i) > \epsilon$. The (refined) action is used to interact with the environment, and the LLM planner is processed in the next step.

(Li et al., 2023a) facilitated cooperation among communicative agents through role-playing and inception prompting, which also includes a critic with different purposes and does not have theoretical guarantees. MetaGPT (Hong et al., 2023) similarly incorporated Standardized Operating Procedures (SOPs) into LLM-based multi-agent collaborations where the roles of each agent was predefined by humans. Compared to previous LLM-based multi-agent works, we propose a more principled way by using the sequential advantage function from multi-agent RL for cooperation.

5 Experiments

We provide the main results and corresponding analysis on the benchmark *DV-RoCoBench* adapted from RoCoBench (Mandi et al., 2023) in this section. The additional results on the adapted *Overcooked-AI* (Carroll et al., 2019) with a detailed setup description in §D.4 are provided in §E.2.

5.1 Experimental Setup

DV-RoCoBench. We present *Difficult Variants of RoCoBench (DV-RoCoBench)* for embodied multi-robot collaboration, which is derived from RoCoBench (Mandi et al., 2023). RoCoBench consists of 6 multi-robot collaboration tasks in a tabletop manipulation environment, typically involving interactive objects that are semantically straightforward to comprehend and reason about for LLMs. In contrast to RoCoBench, which focuses primarily on tasks with a fixed difficulty level, we select three tasks to enrich the complexity of the benchmark and create the new *DV-RoCoBench*, where each task is tailored to have 4-5 difficulty levels for experiments. Due to technically unresolved issues in the original RoCoBench, we have already selected

all executable tasks to form our newly developed *DV-RoCoBench*.

In the following, we give a brief description of tasks and settings. See §D for details.

- **Sweep Floor.** Two robot arms need to work together to sweep all the cubes of given colors into the bin. We establish 5 difficulty levels based on the number of overall cubes and the target cubes.
- **Make Sandwich.** Two robot arms need to stack the ingredients to make a sandwich according to the recipe. Each arm is limited in operating range and cooperation between agents is required. We establish 4 difficulty levels depending on the length of the recipe.
- **Sort Cubes.** Three robot arms within their operating ranges are required to coordinate and place cubes to their target positions. We establish 5 different difficulty levels based on the distance between the cubes and their target locations.

For quantitative comparisons, we impose the maximum number of environment steps per episode to 15 in *DV-RoCoBench*. And the maximum rounds of re-planning per step is set to 15 for all tasks except for Sort Cubes where it is set to 10.

Baseline Methods. We use GPT-4-Turbo (OpenAI, 2023) as the basic LLM policy for all experiments. Since our *ReAd* lies in the setting of LLM grounding on embodied tasks, we mainly choose LLM-based methods as baselines. On both benchmarks, we compare *ReAd-J* with three strong close-loop baselines – ReAct (Yao et al., 2023b), Reflexion (Shinn et al., 2023) and MindAgent (Gong et al., 2023), and a planner named Central Plan which instructs the LLM to generate actions for all robots based on the history of all agents. These five methods output agents’ plans in a parallel manner. In

DV-RoCoBench, we particularly add one more baseline RoCo (Mandi et al., 2023) which achieves the state-of-the-art performance in RoCoBench (Mandi et al., 2023), for comparisons with *ReAd-S*. Both of them generate joint plans in a sequential manner. A detailed comparison among all chosen algorithms is provided in Table 3 of §E.1.

Evaluation Metrics. We evaluate the performance of algorithms on three metrics that closely resemble that in RoCoBench: (i) **SR**: the success rate of completing tasks within the limited interaction rounds; (ii) **ES**: the number of interaction steps to the environment taken by the robots to complete the task; (iii) **NQ**: the number of queries to LLMs in completing the task, which measures the efficiency in enquiring LLMs to obtain a feasible plan. An algorithm is better if it has *higher SR, fewer ES, and fewer NQ*. Among these metrics, SR and ES directly reflect the effectiveness of a planner in completing tasks, while NQ can be somewhat trivial since a planner can have much fewer queries to LLM but has a low SR. In contrast, methods that require policy refinement often require more queries to lead to a high SR.

5.2 Results

***ReAd-S* and *ReAd-J* outperform their corresponding strong baselines on all metrics and achieve more efficient LLM grounding.** As shown in Figure 3, the performance gap in SR becomes pronounced gradually with increasing difficulty level in *DV-RoCoBench*. In more challenging scenarios (e.g., level 4 or 5 in tasks), our approach obtains higher success rates while baselines show limited progress. Meanwhile, *ReAd-S* and *ReAd-J* exhibit lower ES and comparable or even lower NQ across most tasks in *DV-RoCoBench* when compared to their baselines. A lower ES indicates that prompting LLMs to generate actions that maximize advantages can enhance the optimality of the proposed plans, as higher advantages suggest that the generated actions contribute more effectively to task completion. A similar trend is also observed in the result on the adapted *Overcooked-AI* shown in Figure 9. By replacing the *physical verification* feedback with *advantage function*, we implicitly perform one-step monotonic policy improvement over the base LLM in a tuning-free manner, resulting in a stronger LLM planner. On the other hand, as the scenario becomes more challenging for multi-agent collaboration, it is inevitable to involve more redundant information and disturbing

Table 1: Evaluation results over 10 runs of *ReAd-S* and RoCo and its modified versions on disturbances at timestep n . We present the disturbance as resetting the environment. $n = 0$: no resetting.

	Method	NQ	ES	SR
recipe3 ($n = 0$)	ReAd-S	22.1±1.65	8.9±0.28	1.0±0.00
	RoCo-L	44.7±4.90	12.0±0.54	0.9±0.10
	RoCo-P	33.7±3.16	11.5±0.95	0.8±0.13
	RoCo	33.7±3.16	11.5±0.95	0.8±0.13
recipe3 ($n = 1$)	ReAd-S	39.7±5.30	10.4±0.34	1.0±0.00
	RoCo-L	55.3±2.63	14.1±0.28	0.8±0.13
	RoCo-P	33.6±2.03	12.5±0.73	0.9±0.10
	RoCo	46.3±3.60	13.9±0.43	0.7±0.15
recipe3 ($n = 2$)	ReAd-S	44.9±4.34	12.5±0.34	1.0±0.00
	RoCo-L	53.4±2.28	14.8±0.20	0.3±0.15
	RoCo-P	35.2±0.98	14.3±0.26	0.8±0.13
	RoCo	61.2±11.95	14.2±0.44	0.5±0.16
recipe3 ($n = 3$)	ReAd-S	49.1±4.53	13.4±0.54	1.0±0.0
	RoCo-L	75.9±6.91	15.0±0.00	0.0±0.00
	RoCo-P	40.0±2.94	14.3±0.26	0.5±0.17
	RoCo	74.8±10.79	15.0±0.00	0.0±0.00

components in the environment, which poses a challenge for the LLM planner to capture and reason about the essential part inside the state and physical feedback. In contrast, benefiting from *ReAd* feedback, the LLM planner only needs to concentrate on how to maximize the advantage score no matter how challenging the scenario is. Hence, our approach exhibits superior planning capabilities and better LLM grounding results for embodied tasks. Additionally, we evaluate the performance of the open-source model Llama-3.1-70B-Instruct (Dubey et al., 2024) equipped with our algorithm on the *Y2_G3* task. The result is provided in §E.4.

With sudden disturbances towards the environments, the LLM-planner can re-adjust plans rapidly to accomplish the task via *ReAd* feedback. Since the critic takes both the current state and the proposed actions as input, it endows the LLM planner with not only the foresight to discern whether the action contributes to realizing the goal but also the ability to reschedule the planning quickly when encountering sudden disturbances to the advancement of the task. To evaluate the robustness of the LLM planner, we compare *ReAd-S* and RoCo in extra extended scenarios with unexpected disruptions. We select *recipe3* (3rd difficulty level in Make Sandwich) that takes a minimum environment step of 8 to accomplish the task. When a disruption occurs at timestep n ($0 \leq n < 8, n \in \mathbb{N}$), we reset the task and reinitialize the state without giving any hints about this resetting in the prompt and clearing previous history information

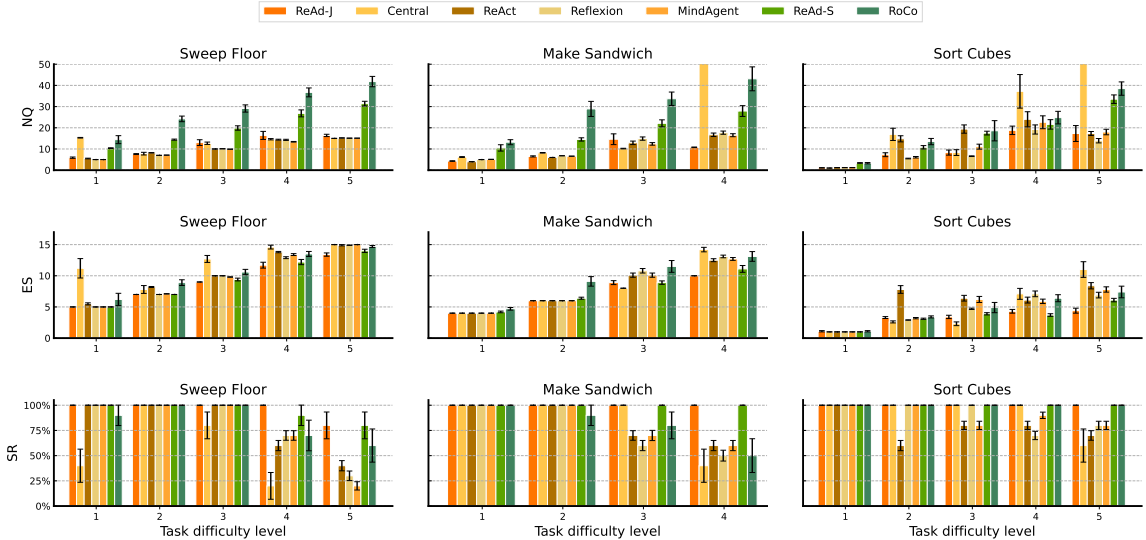


Figure 3: We report mean SR (\uparrow), ES (\downarrow), and NQ (\downarrow) in 3 tasks with various difficulty levels averaged over 10 random seeds. The detailed score is given in Table 4 of §E.3.

contained in the prompt. Specifically, the “adversarial” case affects the LLM-based agent from two aspects: (i) the description of current state s_{reset} which is given to the LLM planner before planning; (ii) the unexpected transition of environment after executing an action. It raises an intractable challenge as the remaining historical information becomes misaligned with the actual situation. The lack of a complete description of the sudden disruption significantly increases the likelihood of the LLM planner proposing erroneous actions. To eliminate the influence induced by the different history information utilized between *ReAd-S* and *RoCo*, we provide two more variants of *RoCo* as baselines. One uses only the history of the previous round, which we name *RoCo-L*, while the other is informed with descriptions of the sudden disturbance, which we name *RoCo-P*. The evaluation results are shown in Table 1. A larger step n signifies a more severe influence of disturbance. As n increases from 0 to 3, *ReAd-S* consistently outperforms *RoCo* and its variants on SR and ES. Although *RoCo* retains a high SR under $n = 1, 2$, it fails to recalibrate the misalignment between the remaining history information and the actual status of the environment, leading to a significant drop in SR when $n = 3$. Regardless of what kind of history information *RoCo* relies on, consistent superior performance demonstrates that *ReAd* feedback alleviates the potentially severe hallucination issue and brings reliable robustness.

5.3 Ablation Studies

Plan refinement has a remarkable impact on grounding LLM. The advantage score plays two

Table 2: The performance of the multi-step and single-step version of *ReAd-S* and *ReAd-J* on the *Y3_G3* task.

	NQ	ES	SR
<i>ReAd-J</i> (Multi-Step)	16.4±0.54	13.4±0.27	0.8±0.13
<i>ReAd-J</i> (Single-Step)	19.1±1.25	14.1±0.28	0.6±0.16
<i>ReAd-S</i> (Multi-Step)	31.4±1.11	14.0±0.26	0.8±0.13
<i>ReAd-S</i> (Single-Step)	35.1±1.16	14.5±0.17	0.6±0.16

roles in *ReAd*: (i) *prompting as optimizing* for generating actions with the highest score, and (ii) *feedback as refinement* for re-plan if the score is less than a threshold. The policy refinement makes our method a *multi-step* process since the action can be refined for multi-rounds. To investigate the role of plan refinement, we adopt a *single-step* version by removing the second role, which forms an open-loop plan generation without refinement. In Table 2, we denote the original version as *Multi-Step* and the open-loop version as *Single-Step*. We pick the most difficult variant *Y3_G3* in Sweep Floor and observe a marginal decline in both efficiency and success rates in *Single-Step*. It suggests that plan refinement that ensures monotonic policy improvement is crucial for performance. Interestingly, *ReAd-J*(*Single-Step*) can also achieve a considerable success rate of 60%, which is dramatically comparable or superior to the baselines with *physical verification* as feedback.

6 Conclusion

We have presented *ReAd* as a novel LLM feedback for closed-loop planning in multi-agent collaboration. We provide theoretical motivation based on multi-agent advantage-weighted regression. The

LLM is prompted to generate plans with high advantages and perform policy refinement. The experiments on *DV-RoCoBench* and *Overcooked-AI* show that our method outperforms physical feedback with improved efficiency. Moreover, the advantage feedback can handle sudden disturbances and is crucial for refinement.

Limitations

Due to the limitation of currently available benchmark for embodied multi-agent collaboration evaluation, most of our experiments are conducted in 2 or 3-agent scenarios. In a case with an increasing number of agents, theoretically speaking, *ReAd-J* would be hindered by the exponential growth of the joint state-action space while *ReAd-S* could maintain consistent performance by scoring in the individual state-action space, enjoying the benefit of sequential decision-making manner. However, it also necessitates more computational costs and time for dataset collection in such a scenario. Thus, how our proposed *ReAd* feedback mechanism practically scales under scenarios with many agents remains fascinating. To this end, building a well-established embodied many-agent collaboration benchmark is essential, which provides an opportunity to push our algorithm to the limit. We consider investigating the *ReAd* feedback mechanism in the many-agent scenario and tackling the potential limitation in future works. Future works also include extending the advantage feedback to multi-objective and safe planning scenarios. Last but not least, we provide extended discussion on Symbol Grounding Problem (Harnad, 1990) in §F.

Acknowledgements

We would like to thank Prof. Zhuoran Yang for his insightful discussions and comments. This work is supported by the National Key Research and Development Program of China (Grant No.2024YFE0210900), the National Natural Science Foundation of China (Grant No.62306242), the Young Elite Scientists Sponsorship Program by CAST (Grant No.2024QNRC001), and the Yangfan Project of the Shanghai (Grant No.23YF11462200).

References

Jacob Abernethy, Alekh Agarwal, Teodor V Marinov, and Manfred K Warmuth. 2023. A mechanism for

sample-efficient in-context learning for sparse retrieval tasks. *arXiv preprint arXiv:2305.17040*.

Michael Ahn, Anthony Brohan, Yevgen Chebotar, Chelsea Finn, Karol Hausman, Alexander Herzog, Daniel Ho, Julian Ibarz, Alex Irpan, Eric Jang, Ryan Julian, Dmitry Kalashnikov, Sergey Levine, and et al. 2022. Do as i can, not as i say: Grounding language in robotic affordances. In *Annual Conference on Robot Learning*.

Ekin Akyürek, Dale Schuurmans, Jacob Andreas, Tengyu Ma, and Denny Zhou. 2023. What learning algorithm is in-context learning? investigations with linear models. In *International Conference on Learning Representations*.

Anthony Brohan, Noah Brown, Justice Carbajal, Yevgen Chebotar, Xi Chen, Krzysztof Choromanski, Tianli Ding, Danny Driess, Avinava Dubey, Chelsea Finn, Pete Florence, Chuyuan Fu, Montse Gonzalez Arenas, Keerthana Gopalakrishnan, Kehang Han, Karol Hausman, Alexander Herzog, and et al. 2023a. RT-2: vision-language-action models transfer web knowledge to robotic control. *CoRR*, abs/2307.15818.

Anthony Brohan, Noah Brown, Justice Carbajal, Yevgen Chebotar, Joseph Dabis, Chelsea Finn, Keerthana Gopalakrishnan, Karol Hausman, Alexander Herzog, and et al. 2023b. Rt-1: Robotics transformer for real-world control at scale. In *Robotics: Science and Systems*.

Tom B. Brown, Benjamin Mann, Nick Ryder, Melanie Subbiah, Jared Kaplan, Prafulla Dhariwal, Arvind Neelakantan, Pranav Shyam, Girish Sastry, Amanda Askell, Sandhini Agarwal, Ariel Herbert-Voss, Gretchen Krueger, Tom Henighan, Rewon Child, Aditya Ramesh, Daniel M. Ziegler, Jeffrey Wu, Clemens Winter, Christopher Hesse, Mark Chen, Eric Sigler, Mateusz Litwin, Scott Gray, Benjamin Chess, Jack Clark, Christopher Berner, Sam McCandlish, Alec Radford, Ilya Sutskever, and Dario Amodei. 2020. Language models are few-shot learners. In *Advances in Neural Information Processing Systems*.

Cameron B Browne, Edward Powley, Daniel Whitehouse, Simon M Lucas, Peter I Cowling, Philipp Rohlfshagen, Stephen Tavener, Diego Perez, Spyridon Samothrakis, and Simon Colton. 2012. A survey of monte carlo tree search methods. *IEEE Transactions on Computational Intelligence and AI in games*, 4(1):1–43.

Micah Carroll, Rohin Shah, Mark K. Ho, Thomas L. Griffiths, Sanjit A. Seshia, Pieter Abbeel, and Anca Dragan. 2019. On the utility of learning about humans for human-ai coordination. *Proceedings of the 33rd International Conference on Neural Information Processing Systems*.

Yongchao Chen, Jacob Arkin, Yang Zhang, Nicholas Roy, and Chuchu Fan. 2023. Scalable multi-robot collaboration with large language models: Centralized or decentralized systems? *CoRR*, abs/2309.15943.

- Aakanksha Chowdhery, Sharan Narang, Jacob Devlin, Maarten Bosma, Gaurav Mishra, Adam Roberts, Paul Barham, Hyung Won Chung, Charles Sutton, Sebastian Gehrmann, et al. 2023. Palm: Scaling language modeling with pathways. *Journal of Machine Learning Research*, 24(240):1–113.
- Open X.-Embodiment Collaboration. 2023. Open x-embodiment: Robotic learning datasets and RT-X models. *CoRR*, abs/2310.08864.
- Josef Dai, Xuehai Pan, Ruiyang Sun, Jiaming Ji, Xinbo Xu, Mickel Liu, Yizhou Wang, and Yaodong Yang. 2023. Safe rlhf: Safe reinforcement learning from human feedback. *arXiv preprint arXiv:2310.12773*.
- Jacob Devlin, Ming-Wei Chang, Kenton Lee, and Kristina Toutanova. 2019. BERT: pre-training of deep bidirectional transformers for language understanding. In *Conference of the North American Chapter of the Association for Computational Linguistics: Human Language Technologies, NAACL-HLT*, pages 4171–4186.
- Qingxiu Dong, Lei Li, Damai Dai, Ce Zheng, Zhiyong Wu, Baobao Chang, Xu Sun, Jingjing Xu, and Zhifang Sui. 2022. A survey for in-context learning. *arXiv preprint arXiv:2301.00234*.
- Danny Driess, Fei Xia, Mehdi S. M. Sajjadi, Corey Lynch, Aakanksha Chowdhery, Brian Ichter, Ayzaan Wahid, Jonathan Tompson, Quan Vuong, Tianhe Yu, Wenlong Huang, Yevgen Chebotar, Pierre Sermanet, Daniel Duckworth, Sergey Levine, Vincent Vanhoucke, Karol Hausman, Marc Toussaint, Klaus Greff, Andy Zeng, Igor Mordatch, and Pete Florence. 2023. Palm-e: An embodied multimodal language model. In *International Conference on Machine Learning*, volume 202, pages 8469–8488.
- Abhimanyu Dubey, Abhinav Jauhri, Abhinav Pandey, Abhishek Kadian, Ahmad Al-Dahle, Aiesha Letman, Akhil Mathur, Alan Schelten, Amy Yang, Angela Fan, et al. 2024. The llama 3 herd of models. *arXiv preprint arXiv:2407.21783*.
- Xidong Feng, Ziyu Wan, Muning Wen, Ying Wen, Weinan Zhang, and Jun Wang. 2023. Alphazero-like tree-search can guide large language model decoding and training. *arXiv preprint arXiv:2309.17179*.
- Patrick Fernandes, Aman Madaan, Emmy Liu, António Farinhas, Pedro Henrique Martins, Amanda Bertsch, José GC de Souza, Shuyan Zhou, Tongshuang Wu, Graham Neubig, et al. 2023. Bridging the gap: A survey on integrating (human) feedback for natural language generation. *arXiv preprint arXiv:2305.00955*.
- Roya Firooz, Johnathan Tucker, Stephen Tian, Anirudha Majumdar, Jiankai Sun, Weiyu Liu, Yuke Zhu, Shuran Song, Ashish Kapoor, Karol Hausman, Brian Ichter, Danny Driess, Jiajun Wu, Cewu Lu, and Mac Schwager. 2023. Foundation models in robotics: Applications, challenges, and the future. *CoRR*, abs/2312.07843.
- Ran Gong, Qiuyuan Huang, Xiaojian Ma, Hoi Vo, Zane Durante, Yusuke Noda, Zilong Zheng, Song-Chun Zhu, Demetri Terzopoulos, Li Fei-Fei, et al. 2023. Mindagent: Emergent gaming interaction. *arXiv preprint arXiv:2309.09971*.
- Yanjiang Guo, Yen-Jen Wang, Lihan Zha, Zheyuan Jiang, and Jianyu Chen. 2023. Doremi: Grounding language model by detecting and recovering from plan-execution misalignment. *arXiv preprint arXiv:2307.00329*.
- Shibo Hao, Yi Gu, Haodi Ma, Joshua Jiahua Hong, Zhen Wang, Daisy Zhe Wang, and Zhiting Hu. 2023. Reasoning with language model is planning with world model. *arXiv preprint arXiv:2305.14992*.
- Stevan Harnad. 1990. The symbol grounding problem. *Physica D: Nonlinear Phenomena*, 42(1-3):335–346.
- Sirui Hong, Xiawu Zheng, Jonathan Chen, Yuheng Cheng, Jinlin Wang, Ceyao Zhang, Zili Wang, Steven Ka Shing Yau, Zijuan Lin, Liyang Zhou, et al. 2023. Metagpt: Meta programming for multi-agent collaborative framework. *arXiv preprint arXiv:2308.00352*.
- Mengkang Hu, Yao Mu, Xinmiao Yu, Mingyu Ding, Shiguang Wu, Wenqi Shao, Qiguang Chen, Bin Wang, Yu Qiao, and Ping Luo. 2023a. Tree-planner: Efficient close-loop task planning with large language models. *arXiv preprint arXiv:2310.08582*.
- Yingdong Hu, Fanqi Lin, Tong Zhang, Li Yi, and Yang Gao. 2023b. Look before you leap: Unveiling the power of gpt-4v in robotic vision-language planning. *arXiv preprint arXiv:2311.17842*.
- Wenlong Huang, Pieter Abbeel, Deepak Pathak, and Igor Mordatch. 2022a. Language models as zero-shot planners: Extracting actionable knowledge for embodied agents. In *International Conference on Machine Learning*, pages 9118–9147. PMLR.
- Wenlong Huang, Chen Wang, Ruohan Zhang, Yunzhu Li, Jiajun Wu, and Li Fei-Fei. 2023. Voxposer: Composable 3d value maps for robotic manipulation with language models. In *Annual Conference on Robot Learning*.
- Wenlong Huang, Fei Xia, Ted Xiao, Harris Chan, Jacky Liang, Pete Florence, Andy Zeng, Jonathan Tompson, Igor Mordatch, Yevgen Chebotar, Pierre Sermanet, Tomas Jackson, Noah Brown, Linda Luu, Sergey Levine, Karol Hausman, and brian ichter. 2022b. Inner monologue: Embodied reasoning through planning with language models. In *Annual Conference on Robot Learning*.
- Sham Kakade and John Langford. 2002. Approximately optimal approximate reinforcement learning. In *International Conference on Machine Learning*, page 267–274.
- Shyam Sundar Kannan, Vishnunandan L. N. Venkatesh, and Byung-Cheol Min. 2023. Smart-llm: Smart multi-agent robot task planning using large language models. *CoRR*, abs/2309.10062.

- Jakub Grudzien Kuba, Ruiqing Chen, Muning Wen, Ying Wen, Fanglei Sun, Jun Wang, and Yaodong Yang. 2022a. Trust region policy optimisation in multi-agent reinforcement learning. In *International Conference on Learning Representations, ICLR*.
- Jakub Grudzien Kuba, Xidong Feng, Shiyao Ding, Hao Dong, Jun Wang, and Yaodong Yang. 2022b. Heterogeneous-agent mirror learning: A continuum of solutions to cooperative MARL. *CoRR*, abs/2208.01682.
- Harold W. Kuhn and Albert W. Tucker. 1950. Nonlinear programming. In *Berkeley Symposium on Mathematical Statistics and Probability*, page 481–492.
- Sergey Levine, Aviral Kumar, George Tucker, and Justin Fu. 2020. Offline reinforcement learning: Tutorial, review, and perspectives on open problems. *arXiv preprint arXiv:2005.01643*.
- Guohao Li, Hasan Hammoud, Hani Itani, Dmitrii Khizbullin, and Bernard Ghanem. 2023a. Camel: Communicative agents for "mind" exploration of large language model society. *Advances in Neural Information Processing Systems*, 36:51991–52008.
- Xinghang Li, Minghuan Liu, Hanbo Zhang, Cunjun Yu, Jie Xu, Hongtao Wu, Chilam Cheang, Ya Jing, Weinan Zhang, Huaping Liu, Hang Li, and Tao Kong. 2023b. Vision-language foundation models as effective robot imitators. *CoRR*, abs/2311.01378.
- Jacky Liang, Wenlong Huang, Fei Xia, Peng Xu, Karol Hausman, Brian Ichter, Pete Florence, and Andy Zeng. 2023. Code as policies: Language model programs for embodied control. In *IEEE International Conference on Robotics and Automation*, pages 9493–9500. IEEE.
- Bill Yuchen Lin, Yicheng Fu, Karina Yang, Faeze Brahman, Shiyu Huang, Chandra Bhagavatula, Prithviraj Ammanabrolu, Yejin Choi, and Xiang Ren. 2023a. Swiftsage: A generative agent with fast and slow thinking for complex interactive tasks. In *Neural Information Processing Systems*.
- Bill Yuchen Lin, Chengsong Huang, Qian Liu, Wenda Gu, Sam Sommerer, and Xiang Ren. 2023b. On grounded planning for embodied tasks with language models. In *AAAI Conference on Artificial Intelligence*, volume 37, pages 13192–13200.
- Jessy Lin, Yuqing Du, Olivia Watkins, Danijar Hafner, Pieter Abbeel, Dan Klein, and Anca Dragan. 2023c. Learning to model the world with language. *arXiv preprint arXiv:2308.01399*.
- Kevin Lin, Christopher Agia, Toki Migimatsu, Marco Pavone, and Jeannette Bohg. 2023d. Text2motion: from natural language instructions to feasible plans. *Auton. Robots*, 47(8):1345–1365.
- Bo Liu, Yuqian Jiang, Xiaohan Zhang, Qiang Liu, Shiqi Zhang, Joydeep Biswas, and Peter Stone. 2023a. Llm+ p: Empowering large language models with optimal planning proficiency. *arXiv preprint arXiv:2304.11477*.
- Zhihan Liu, Hao Hu, Shenao Zhang, Hongyi Guo, Shuqi Ke, Boyi Liu, and Zhaoran Wang. 2023b. Reason for future, act for now: A principled architecture for autonomous llm agents. In *NeurIPS 2023 Foundation Models for Decision Making Workshop*.
- Yecheng Jason Ma, William Liang, Guanzhi Wang, De-An Huang, Osbert Bastani, Dinesh Jayaraman, Yuke Zhu, Linxi Fan, and Anima Anandkumar. 2023. Eureka: Human-level reward design via coding large language models. *CoRR*, abs/2310.12931.
- Zhao Mandi, Shreeya Jain, and Shuran Song. 2023. Roco: Dialectic multi-robot collaboration with large language models. *CoRR*, abs/2307.04738.
- Yao Mu, Qinglong Zhang, Mengkang Hu, Wenhai Wang, Mingyu Ding, Jun Jin, Bin Wang, Jifeng Dai, Yu Qiao, and Ping Luo. 2023. EmbodiedGPT: Vision-language pre-training via embodied chain of thought. In *Neural Information Processing Systems*.
- Rithesh Murthy, Shelby Heinecke, Juan Carlos Niebles, Zhiwei Liu, Le Xue, Weiran Yao, Yihao Feng, Zeyuan Chen, Akash Gokul, Devansh Arpit, et al. 2023. Rex: Rapid exploration and exploitation for ai agents. *arXiv preprint arXiv:2307.08962*.
- OpenAI. 2023. Gpt-4 technical report.
- Xue Bin Peng, Aviral Kumar, Grace Zhang, and Sergey Levine. 2019. Advantage-weighted regression: Simple and scalable off-policy reinforcement learning. *CoRR*, abs/1910.00177.
- Alec Radford, Jeffrey Wu, Rewon Child, David Luan, Dario Amodei, Ilya Sutskever, et al. 2019. Language models are unsupervised multitask learners. *OpenAI blog*, 1(8):9.
- Colin Raffel, Noam Shazeer, Adam Roberts, Katherine Lee, Sharan Narang, Michael Matena, Yanqi Zhou, Wei Li, and Peter J. Liu. 2020. Exploring the limits of transfer learning with a unified text-to-text transformer. *Journal of Machine Learning Research*, 21:140:1–140:67.
- Tabish Rashid, Mikayel Samvelyan, Christian Schroeder de Witt, Gregory Farquhar, Jakob Foerster, and Shimon Whiteson. 2020. Monotonic value function factorisation for deep multi-agent reinforcement learning. *Journal of Machine Learning Research*, 21(178):1–51.
- John Schulman, Sergey Levine, Pieter Abbeel, Michael Jordan, and Philipp Moritz. 2015. Trust region policy optimization. In *International Conference on Machine Learning*, pages 1889–1897.
- Noah Shinn, Federico Cassano, Edward Berman, Ashwin Gopinath, Karthik Narasimhan, and Shunyu Yao. 2023. Reflexion: Language agents with verbal reinforcement learning. In *Neural Information Processing Systems*.

- Tom Silver, Soham Dan, Kavitha Srinivas, Joshua B Tenenbaum, Leslie Pack Kaelbling, and Michael Katz. 2023. Generalized planning in pddl domains with pretrained large language models. *arXiv preprint arXiv:2305.11014*.
- Chan Hee Song, Jiaman Wu, Clayton Washington, Brian M. Sadler, Wei-Lun Chao, and Yu Su. 2023a. Llm-planner: Few-shot grounded planning for embodied agents with large language models. In *IEEE/CVF International Conference on Computer Vision (ICCV)*.
- Feifan Song, Bowen Yu, Minghao Li, Haiyang Yu, Fei Huang, Yongbin Li, and Houfeng Wang. 2023b. Preference ranking optimization for human alignment. *arXiv preprint arXiv:2306.17492*.
- Hugo Touvron, Thibaut Lavril, Gautier Izacard, Xavier Martinet, Marie-Anne Lachaux, Timothée Lacroix, Baptiste Rozière, Naman Goyal, Eric Hambro, Faisal Azhar, et al. 2023a. Llama: Open and efficient foundation language models. *arXiv preprint arXiv:2302.13971*.
- Hugo Touvron, Louis Martin, Kevin Stone, Peter Albert, Amjad Almahairi, Yasmine Babaei, Nikolay Bashlykov, Soumya Batra, Prajjwal Bhargava, Shruti Bhosale, et al. 2023b. Llama 2: Open foundation and fine-tuned chat models. *arXiv preprint arXiv:2307.09288*.
- Sai Vemprala, Rogerio Bonatti, Arthur Bucker, and Ashish Kapoor. 2023. Chatgpt for robotics: Design principles and model abilities. *Microsoft Auton. Syst. Robot. Res*, 2:20.
- Lirui Wang, Yiyang Ling, Zhecheng Yuan, Mohit Shridhar, Chen Bao, Yuzhe Qin, Bailin Wang, Huazhe Xu, and Xiaolong Wang. 2023a. Gensim: Generating robotic simulation tasks via large language models. *CoRR*, abs/2310.01361.
- Yen-Jen Wang, Bike Zhang, Jianyu Chen, and Koushil Sreenath. 2023b. Prompt a robot to walk with large language models. *CoRR*, abs/2309.09969.
- Yufei Wang, Zhou Xian, Feng Chen, Tsun-Hsuan Wang, Yian Wang, Zackory Erickson, David Held, and Chuang Gan. 2023c. Robogen: Towards unleashing infinite data for automated robot learning via generative simulation. *CoRR*, abs/2311.01455.
- Jason Wei, Xuezhi Wang, Dale Schuurmans, Maarten Bosma, brian ichter, Fei Xia, Ed H. Chi, Quoc V Le, and Denny Zhou. 2022. Chain of thought prompting elicits reasoning in large language models. In *Advances in Neural Information Processing Systems*.
- Zhenyu Wu, Ziwei Wang, Xiuwei Xu, Jiwen Lu, and Haibin Yan. 2023. Embodied task planning with large language models. *arXiv preprint arXiv:2307.01848*.
- Tengyang Xie, Ching-An Cheng, Nan Jiang, Paul Mineiro, and Alekh Agarwal. 2021. Bellman-consistent pessimism for offline reinforcement learning. *Advances in neural information processing systems*, 34:6683–6694.
- Tianbao Xie, Siheng Zhao, Chen Henry Wu, Yitao Liu, Qian Luo, Victor Zhong, Yanchao Yang, and Tao Yu. 2023a. Text2reward: Automated dense reward function generation for reinforcement learning. *CoRR*, abs/2309.11489.
- Yuxi Xie, Kenji Kawaguchi, Yiran Zhao, Xu Zhao, Min-Yen Kan, Junxian He, and Qizhe Xie. 2023b. Self-evaluation guided beam search for reasoning. In *Thirty-seventh Conference on Neural Information Processing Systems*.
- Runsen Xu, Xiaolong Wang, Tai Wang, Yilun Chen, Jiangmiao Pang, and Dahua Lin. 2023. Pointllm: Empowering large language models to understand point clouds. *arXiv preprint arXiv:2308.16911*.
- Chengrun Yang, Xuezhi Wang, Yifeng Lu, Hanxiao Liu, Quoc V. Le, Denny Zhou, and Xinyun Chen. 2023. Large language models as optimizers. *Preprint*, arXiv:2309.03409.
- Shunyu Yao, Dian Yu, Jeffrey Zhao, Izhak Shafran, Thomas L. Griffiths, Yuan Cao, and Karthik R Narasimhan. 2023a. Tree of thoughts: Deliberate problem solving with large language models. In *Neural Information Processing Systems*.
- Shunyu Yao, Jeffrey Zhao, Dian Yu, Nan Du, Izhak Shafran, Karthik R Narasimhan, and Yuan Cao. 2023b. React: Synergizing reasoning and acting in language models. In *International Conference on Learning Representations*.
- Wenhao Yu, Nimrod Gileadi, Chuyuan Fu, Sean Kirmani, Kuang-Huei Lee, Montse Gonzalez Arenas, Hao-Tien Lewis Chiang, Tom Erez, Leonard Hasenclever, Jan Humplik, Brian Ichter, Ted Xiao, Peng Xu, Andy Zeng, Tingnan Zhang, Nicolas Heess, Dorsa Sadigh, Jie Tan, Yuval Tassa, and Fei Xia. 2023. Language to rewards for robotic skill synthesis. *CoRR*, abs/2306.08647.
- Andy Zeng, Maria Attarian, brian ichter, Krzysztof Marcin Choromanski, Adrian Wong, Stefan Welker, Federico Tombari, Aveek Purohit, Michael S Ryoo, Vikas Sindhwani, Johnny Lee, Vincent Vanhoucke, and Pete Florence. 2023. Socratic models: Composing zero-shot multimodal reasoning with language. In *International Conference on Learning Representations*.
- Ceyao Zhang, Kaijie Yang, Siyi Hu, Zihao Wang, Guanghe Li, Yihang Sun, Cheng Zhang, Zhaowei Zhang, Anji Liu, Song-Chun Zhu, et al. 2023a. Proagent: Building proactive cooperative ai with large language models. *arXiv preprint arXiv:2308.11339*.
- Danyang Zhang, Lu Chen, Situo Zhang, Hongshen Xu, Zihan Zhao, and Kai Yu. 2023b. Large language

models are semi-parametric reinforcement learning agents. In *Neural Information Processing Systems*.

Hongxin Zhang, Weihua Du, Jiaming Shan, Qinhong Zhou, Yilun Du, Joshua Tenenbaum, Tianmin Shu, and Chuang Gan. 2023c. Building cooperative embodied agents modularly with large language models. In *NeurIPS 2023 Foundation Models for Decision Making Workshop*.

Kaiqing Zhang, Zhuoran Yang, and Tamer Başar. 2021. Multi-agent reinforcement learning: A selective overview of theories and algorithms. *Studies in Systems, Decision and Control*, 325:321 – 384.

Zirui Zhao, Wee Sun Lee, and David Hsu. 2023. Large language models as commonsense knowledge for large-scale task planning. *arXiv preprint arXiv:2305.14078*.

Zhehua Zhou, Jiayang Song, Kunpeng Yao, Zhan Shu, and Lei Ma. 2023. Isr-llm: Iterative self-refined large language model for long-horizon sequential task planning. *arXiv preprint arXiv:2308.13724*.

A Theoretical Proof

A.1 Derivation of Joint Advantage Function with Joint Action WAIT

The state-action value function with respect to the joint action WAIT \mathbf{w} can be expressed by,

$$\begin{aligned} Q_{\pi}(s, \mathbf{w}) &= \mathbb{E}_{s_{1:\infty} \sim P, \mathbf{a}_{1:\infty} \sim \pi} \left[\sum_{i=0}^{\infty} \gamma^i r_i \mid s_0 = s, \mathbf{a}_0 = \mathbf{w} \right] \\ &= \gamma \mathbb{E}_{s_{2:\infty} \sim P, \mathbf{a}_{1:\infty} \sim \pi} \left[\sum_{i=0}^{\infty} \gamma^i r_{i+1} \mid s_1 = s \right] \\ &= \gamma V_{\pi}(s). \end{aligned}$$

Therefore, the *joint* advantage function can be derived by using only the Q_{π} function, as

$$\begin{aligned} A_{\pi}(s, \mathbf{a}) &= Q_{\pi}(s, \mathbf{a}) - V_{\pi}(s) \\ &= Q_{\pi}(s, \mathbf{a}) - \frac{1}{\gamma} Q_{\pi}(s, \mathbf{w}). \end{aligned}$$

A.2 Proof of Multi-Agent Advantage Decomposition

Proof. With the definition of the multi-agent local advantage function in Eq. (3), we can have

$$\begin{aligned} \sum_{k=1}^n A_{\pi}^{i_k}(s, \mathbf{a}^{i_{1:k-1}}, a^{i_k}) &= \sum_{k=1}^n Q_{\pi}^{i_{1:k}}(s, \mathbf{a}^{i_{1:k}}) - Q_{\pi}^{i_{1:k-1}}(s, \mathbf{a}^{i_{1:k-1}}) \\ &= Q_{\pi}^{i_{1:n}}(s, \mathbf{a}^{i_{1:n}}) - Q_{\pi}^{i_{1:n-1}}(s, \mathbf{a}^{i_{1:n-1}}) + Q_{\pi}^{i_{1:n-1}}(s, \mathbf{a}^{i_{1:n-1}}) - Q_{\pi}^{i_{1:n-2}}(s, \mathbf{a}^{i_{1:n-2}}) \\ &\quad + \dots + Q_{\pi}^{i_{1:1}}(s, \mathbf{a}^{i_{1:1}}) - Q_{\pi}^{i_{1:0}}(s, \mathbf{a}^{i_{1:0}}) \\ &= Q_{\pi}^{i_{1:n}}(s, \mathbf{a}^{i_{1:n}}) - Q_{\pi}^{i_{1:0}}(s, \mathbf{a}^{i_{1:0}}) \\ &= Q_{\pi}(s, \mathbf{a}) - V_{\pi}(s) \\ &= A_{\pi}(s, \mathbf{a}). \end{aligned}$$

□

A.3 Derivation of Optimal Joint Policy and Optimal Individual Policy

In this section, we begin with the constrained policy search problem. Following the performance difference lemma (Kakade and Langford, 2002), the expected improvement $\eta(\pi) = J(\pi) - J(\mu)$ can be expressed by

$$\begin{aligned} \mathbb{E}_{s_0, \mathbf{a}_0, \dots \sim \pi} \left[\sum_{t=0}^{\infty} \gamma^t A_{\mu}(s_t, \mathbf{a}_t) \right] &= \mathbb{E}_{s_0, \mathbf{a}_0, \dots \sim \pi} \left[\sum_{t=0}^{\infty} \gamma^t (r(s_t, \mathbf{a}_t) + \gamma V_{\mu}(s_{t+1}) - V_{\mu}(s_t)) \right] \\ &= \mathbb{E}_{s_0, \mathbf{a}_0, \dots \sim \pi} \left[-V_{\mu}(s_0) + \sum_{t=0}^{\infty} \gamma^t r(s_t, \mathbf{a}_t) \right] \\ &= -\mathbb{E}_{s_0 \sim p(s_0)} [V_{\mu}(s_0)] + \mathbb{E}_{s_0, \mathbf{a}_0, \dots \sim \pi} \left[\sum_{t=0}^{\infty} \gamma^t r(s_t, \mathbf{a}_t) \right] \\ &= -J(\mu) + J(\pi). \end{aligned} \tag{9}$$

We can rewrite Eq. (9) with an expectation over states using discounted visitation frequencies $\rho_{\pi}(s)$,

$$\begin{aligned} \eta(\pi) &= \mathbb{E}_{s_0, \mathbf{a}_0, \dots \sim \pi} \left[\sum_{t=0}^{\infty} \gamma^t A_{\mu}(s_t, \mathbf{a}_t) \right] = \sum_{t=0}^{\infty} \int_s p(s_t = s | \pi) \int_{\mathbf{a}} \pi(\mathbf{a} | s) \gamma^t A_{\mu}(s, \mathbf{a}) d\mathbf{a} ds \\ &= \int_s \sum_{t=0}^{\infty} \gamma^t p(s_t = s | \pi) \int_{\mathbf{a}} \pi(\mathbf{a} | s) A_{\mu}(s, \mathbf{a}) d\mathbf{a} ds \\ &= \int_s \rho_{\pi}(s) \int_{\mathbf{a}} \pi(\mathbf{a} | s) A_{\mu}(s, \mathbf{a}) d\mathbf{a} ds, \end{aligned} \tag{10}$$

where $\rho_\pi(s) = \sum_{t=0}^{\infty} \gamma^t p(s_t = s | \pi)$ represents the (unnormalized) discounted visitation frequencies over policy π and $p(s_t = s | \pi)$ is the likelihood of the agent at state s after following π for t timesteps. Our goal is to find the optimal policy π^* that maximizes the expected improvement $\eta(\pi)$.

However, it's intractable to sample over the target policy π , further causing that the objective in Eq. (10) can be difficult to optimize. Following (Schulman et al., 2015), we can introduce an approximation $\hat{\eta}(\pi)$ of $\eta(\pi)$ using the discounted visitation frequencies over the old policy μ ,

$$\hat{\eta}(\pi) = \int_s \rho_\mu(s) \int_a \pi(\mathbf{a}|s) A_\mu(s, \mathbf{a}) d\mathbf{a} ds.$$

$\hat{\eta}(\pi)$ matches $\eta(\pi)$ to first order (Kakade and Langford, 2002), and provides a good estimate of η if π is close enough to μ . In practice, we initialize the target policy π with the LLM policy μ to satisfy the above condition. Therefore, we can formulate the following constrained policy search problem,

$$\arg \max_{\pi} \int_s \rho_\mu(s) \int_a \pi(\mathbf{a}|s) A_\mu(s, \mathbf{a}) d\mathbf{a} ds, \quad (11)$$

$$\text{s.t. } D_{\text{KL}}(\pi(\cdot|s) \| \mu(\cdot|s)) \leq \epsilon, \quad \forall s, \quad (12)$$

$$\int_a \pi(\mathbf{a}|s) d\mathbf{a} = 1, \quad \forall s. \quad (13)$$

However, enforcing the pointwise KL constraint in Eq. (12) at all states is intractable. To simplify the constrained optimization problem, we relax the hard KL constraint by converting it into a soft constraint in an expectation form, as

$$\arg \max_{\pi} \int_s \rho_\mu(s) \int_a \pi(\mathbf{a}|s) A_\mu(s, \mathbf{a}) d\mathbf{a} ds,$$

$$\text{s.t. } \int_s \rho_\mu(s) D_{\text{KL}}(\pi(\cdot|s) \| \mu(\cdot|s)) ds \leq \epsilon,$$

$$\int_a \pi(\mathbf{a}|s) d\mathbf{a} = 1, \quad \forall s.$$

Next, we form the Lagrangian, as

$$\mathcal{L}(\pi, \beta, \nu) = \int_s \rho_\mu(s) \int_a \pi(\mathbf{a}|s) A_\mu(s, \mathbf{a}) d\mathbf{a} ds + \beta \left(\epsilon - \int_s \rho_\mu(s) D_{\text{KL}}(\pi(\cdot|s) \| \mu(\cdot|s)) ds \right) + \int_s \nu_s \left(1 - \int_a \pi(\mathbf{a}|s) d\mathbf{a} \right) ds,$$

where $\nu = \{\nu_s | \forall s \in \mathcal{S}\}$ and $\beta > 0$ correspond to the Lagrange multipliers.

Derivation of Optimal Joint Policy. Differentiating $\mathcal{L}(\pi, \beta, \nu)$ with respect to $\pi(\mathbf{a}|s)$ gives the following,

$$\frac{\partial \mathcal{L}}{\partial \pi(\mathbf{a}|s)} = \rho_\mu(s) A_\mu(s, \mathbf{a}) - \beta \rho_\mu(s) \log \pi(\mathbf{a}|s) + \beta \rho_\mu(s) \log \mu(\mathbf{a}|s) - \beta \rho_\mu(s) - \nu_s. \quad (14)$$

According to KKT conditions (Kuhn and Tucker, 1950), if (π^*, β^*, ν^*) is a saddle point of \mathcal{L} , π^* is the optimal solution of the primal problem. Thus, let Eq. (14) be equal to zero, then we have

$$\log \pi^*(\mathbf{a}|s) = \frac{1}{\beta^*} A_\mu(s, \mathbf{a}) + \log \mu(\mathbf{a}|s) - 1 - \frac{1}{\rho_\mu(s)} \frac{\nu_s^*}{\beta^*}, \quad (15)$$

$$\pi^*(\mathbf{a}|s) = \mu(\mathbf{a}|s) \exp\left(\frac{1}{\beta^*} A_\mu(s, \mathbf{a})\right) \exp\left(-\frac{1}{\rho_\mu(s)} \frac{\nu_s^*}{\beta^*} - 1\right). \quad (16)$$

Note that the primal problem holds the constraint $\int_{\mathbf{a}} \boldsymbol{\pi}(\mathbf{a}|s) d\mathbf{a} = 1$, the second exponential term is consequently viewed as the partition function $Z(s)$ that normalizes the conditional action distribution,

$$Z(s) = \exp\left(\frac{1}{\rho_{\boldsymbol{\mu}}(s)} \frac{\nu_s^*}{\beta^*} + 1\right) = \int_{\mathbf{a}'} \boldsymbol{\mu}(\mathbf{a}'|s) \exp\left(\frac{1}{\beta^*} A_{\boldsymbol{\mu}}(s, \mathbf{a}')\right) d\mathbf{a}'. \quad (17)$$

Optimal Joint Policy is then given by,

$$\underbrace{\boldsymbol{\pi}^*(\mathbf{a}|s)}_{\text{Left-Hand Side}} = \underbrace{\frac{1}{Z(s)} \boldsymbol{\mu}(\mathbf{a}|s) \exp\left(\frac{1}{\beta^*} A_{\boldsymbol{\mu}}(s, \mathbf{a})\right)}_{\text{Right-Hand Side}}. \quad (18)$$

Derivation of Optimal Individual Policy. Given the set of agents $\mathcal{N} = \{1, 2, \dots, n\}$, we assume the agents choose actions sequentially in the order of $1, 2, \dots, n$, i.e., agents i is aware of current state s and the chosen actions of agents $1, 2, \dots, i-1$ and select actions based on that. The following equation holds by the support of the definition of conditional probability,

$$\boldsymbol{\pi}(\mathbf{a}|s) = \prod_{i=1}^n \pi^i(a^i|s, \mathbf{a}^{1:i-1}), \quad (19)$$

where π^i is the individual policy of agent i . Here we consider a general case that the old joint policy and the target joint policy are both in a sequential manner. Following multi-agent advantage decomposition in Lemma 1, the LHS and RHS of Eq. (18) can be expressed respectively (in order to present the *Optimal Individual Policy* we omit the superscript of it which denotes agent id),

$$\text{LHS} = \prod_{i=1}^n \pi^*(a^i|s, \mathbf{a}^{1:i-1}), \quad (20)$$

$$\begin{aligned} \text{RHS} &= \frac{1}{Z(s)} \prod_{i=1}^n \mu^i(a^i|s, \mathbf{a}^{1:i-1}) \exp\left(\frac{1}{\beta^*} A_{\boldsymbol{\mu}}^i(s, \mathbf{a}^{1:i-1}, a^i)\right) \\ &= \prod_{i=1}^n \frac{1}{Z^i(s)} \mu^i(a^i|s, \mathbf{a}^{1:i-1}) \exp\left(\frac{1}{\beta^*} A_{\boldsymbol{\mu}}^i(s, \mathbf{a}^{1:i-1}, a^i)\right). \end{aligned} \quad (21)$$

Thus, we can get the expression of *Optimal Individual Policy*,

$$\pi^*(a^i|s, \mathbf{a}^{1:i-1}) = \frac{1}{Z^i(s)} \mu^i(a^i|s, \mathbf{a}^{1:i-1}) \exp\left(\frac{1}{\beta^*} A_{\boldsymbol{\mu}}^i(s, \mathbf{a}^{1:i-1}, a^i)\right), \quad (22)$$

where $Z^i(s)$ is the partition function that normalizes the conditional action distribution $\pi^*(a^i|s, \mathbf{a}^{1:i-1})$ of agent i and satisfies $Z(s) = \prod_{i=1}^n Z^i(s)$. Finally, all that remains for us to do is to derive the validity of $Z(s) = \prod_{i=1}^n Z^i(s)$.

Since $Z^i(s)$ is the partition function that normalizes the conditional action distribution $\pi^*(a^i|s, \mathbf{a}^{1:i-1})$, we can have,

$$Z^i(s) = \int_{a^i} \mu^i(a^i|s, \mathbf{a}^{1:i-1}) \exp\left(\frac{1}{\beta^*} A_{\boldsymbol{\mu}}^i(s, \mathbf{a}^{1:i-1}, a^i)\right) da^i. \quad (23)$$

Meanwhile, we can rewrite Eq. (17) after applying multi-agent advantage decomposition in Lemma 1,

$$Z(s) = \int_{\mathbf{a}} \boldsymbol{\mu}(\mathbf{a}|s) \exp\left(\frac{1}{\beta^*} A_{\boldsymbol{\mu}}(s, \mathbf{a})\right) d\mathbf{a} \quad (24)$$

$$= \prod_{i=1}^n \int_{a^i} \mu^i(a^i|s, \mathbf{a}^{1:i-1}) \exp\left(\frac{1}{\beta^*} A_{\boldsymbol{\mu}}^i(s, \mathbf{a}^{1:i-1}, a^i)\right) da^i \quad (25)$$

$$= \prod_{i=1}^n Z^i(s). \quad (26)$$

Beyond the general case, if we consider a special case that the old policy $\boldsymbol{\mu}$ is in a parallel manner (i.e., $\boldsymbol{\mu} = \prod_{i=1}^n \mu^i(a^i|s)$) while the target policy remains in a sequential manner, we can still derive similar results, differing only by the modification from $\mu^i(a^i|s, \mathbf{a}^{1:i-1})$ to $\mu^i(a^i|s)$.

A.4 Proof of Monotonic Improvement with Binary Filtering

Proposition 1. (*Relationship between Exponential Weighting and Binary Filtering*). In terms of the weight $e^{A_{\mu}^i(s, \mathbf{a}^{1:i-1}, a^i)/\beta}$ in Exponential Weighting where $\beta > 0$, for any $A_{\mu}^i(s, \mathbf{a}^{1:i-1}, a^i) < 0$, we have the following limitation,

$$\lim_{\beta \rightarrow 0^+} \exp\left(\frac{A_{\mu}^i(s, \mathbf{a}^{1:i-1}, a^i)}{\beta}\right) = 0, \quad \text{for } \forall A_{\mu}^i(s, \mathbf{a}^{1:i-1}, a^i) < 0 \quad (27)$$

As $\beta \rightarrow 0^+$, Exponential Weighting becomes a special case – Binary Filtering where the samples with $A_{\mu}^i(s, \mathbf{a}^{1:i-1}, a^i) < 0$ are filtered out.

Proof. We first define the minimum of the absolute value of those negative A_{μ}^i ,

$$\alpha = \min_{A_{\mu}^i < 0} |A_{\mu}^i| = \min_{A_{\mu}^i < 0} -A_{\mu}^i$$

To achieve Eq. (27), we only need to ensure that the rate at which $e^{A_{\mu}^i(s, \mathbf{a}^{1:i-1}, a^i)/\beta}$ approaches zero is faster than the rate at which β approaches zero. One way to guarantee this is to choose β such that it is proportional to the absolute value of A . Thus, we define $\beta = k \cdot \alpha$ where k is a positive hyperparameter. Then we have,

$$\exp\left(\frac{A_{\mu}^i(s, \mathbf{a}^{1:i-1}, a^i)}{\beta}\right) \leq \exp\left(\frac{-\alpha}{\beta}\right) = \exp\left(\frac{-1}{k}\right)$$

Finally, for any positive $\epsilon > 0$, there exists a positive $k > 0$, it holds the following:

$$\exp\left(\frac{-1}{k}\right) < \epsilon$$

Taking the natural logarithm of both sides, we get:

$$k \ln(\epsilon) + 1 > 0 \quad (28)$$

With an arbitrary $\epsilon > 0$, we can always find a k that satisfies Eq. (28), further satisfying Eq. (27). \square

Proposition 2. (*Policy improvement with Binary Filtering*). By behaviour cloning (BC) on a filtered dataset with Binary Filtering $\mathbb{1}[A_{\mu}^i(s, \mathbf{a}^{1:i-1}, a^i) > \epsilon]$ where $\epsilon \geq 0$, new policy π is superior to the basic policy μ , i.e., $J(\pi) - J(\mu) > 0$.

Proof. According to BC on a filtered dataset with Binary Filtering $\mathbb{1}[A_{\mu}^i(s, \mathbf{a}^{1:i-1}, a^i) > \epsilon]$, we have:

$$\pi^i(a^i | s, \mathbf{a}^{1:i-1}) = \frac{\mathbb{1}[A_{\mu}^i(s, \mathbf{a}^{1:i-1}, a^i) > \epsilon] \mu^i(a^i | s, \mathbf{a}^{1:i-1})}{Z^i(s)} \quad (29)$$

where $Z^i(s)$ is the partition function. Given the new policy $\pi(\mathbf{a} | s) = \prod_{i=1}^n \pi^i(a^i | s, \mathbf{a}^{1:i-1})$, the expected improvement from Eq. (6) can be rewritten as,

$$\begin{aligned} \hat{\eta}(\pi) &= \mathbb{E}_{s \sim \rho_{\mu}(s), \mathbf{a} \sim \pi(\mathbf{a} | s)} [A_{\mu}(s, \mathbf{a})] \\ &= \mathbb{E}_{s \sim \rho_{\mu}(s)} \mathbb{E}_{a^1 \sim \pi^1(a^1 | s)} \mathbb{E}_{a^2 \sim \pi^2(a^2 | s, a^1)} \cdots \mathbb{E}_{a^n \sim \pi^n(a^n | s, \mathbf{a}^{1:n-1})} [A_{\mu}(s, \mathbf{a})] \end{aligned}$$

Substituting Lemma 1 and Eq. (29) into the above equation, we get:

$$\begin{aligned} \hat{\eta}(\pi) &= \mathbb{E}_{s \sim \rho_{\mu}(s)} \mathbb{E}_{a^1 \sim \pi^1(a^1 | s)} \mathbb{E}_{a^2 \sim \pi^2(a^2 | s, a^1)} \cdots \mathbb{E}_{a^n \sim \pi^n(a^n | s, \mathbf{a}^{1:n-1})} \left[\sum_{i=1}^n A_{\mu}^i(s, \mathbf{a}^{1:i-1}, a^i) \right] \\ &= \mathbb{E}_{s \sim \rho_{\mu}(s)} \left[\sum_{i=1}^n \mathbb{E}_{a^i \sim \pi^i(a^i | s, \mathbf{a}^{1:i-1})} (A_{\mu}^i(s, \mathbf{a}^{1:i-1}, a^i)) \right] \\ &= \mathbb{E}_{s \sim \rho_{\mu}(s)} \left[\sum_{i=1}^n \mathbb{E}_{a^i \sim \mu^i(a^i | s, \mathbf{a}^{1:i-1})} \left(\frac{\mathbb{1}[A_{\mu}^i(s, \mathbf{a}^{1:i-1}, a^i) > \epsilon] A_{\mu}^i(s, \mathbf{a}^{1:i-1}, a^i)}{Z^i(s)} \right) \right] \quad (30) \end{aligned}$$

And we note that the expected improvement from Eq. (6) entails the following relationship,

$$\begin{aligned}
\hat{\eta}(\boldsymbol{\mu}) &= J(\boldsymbol{\mu}) - J(\boldsymbol{\mu}) = \mathbb{E}_{s \sim \rho_{\boldsymbol{\mu}}(s), \mathbf{a} \sim \boldsymbol{\mu}(\mathbf{a}|s)} [A_{\boldsymbol{\mu}}(s, \mathbf{a})] \\
&= \mathbb{E}_{s \sim \rho_{\boldsymbol{\mu}}(s)} \left[\sum_{i=1}^n \mathbb{E}_{a^i \sim \mu^i(a^i|s, \mathbf{a}^{1:i-1})} (A_{\boldsymbol{\mu}}^i(s, \mathbf{a}^{1:i-1}, a^i)) \right] \\
&= 0
\end{aligned} \tag{31}$$

Comparing Eq. (30) with Eq. (31), it is obvious that those local advantages $A_{\boldsymbol{\mu}}^i(s, \mathbf{a}^{1:i-1}, a^i)$ below the threshold ϵ would not be calculated in the expectation $\hat{\eta}(\boldsymbol{\pi})$. Hence, when the threshold $\epsilon \geq 0$ it naturally holds $\hat{\eta}(\boldsymbol{\pi}) > \hat{\eta}(\boldsymbol{\mu}) = 0$, i.e., $J(\boldsymbol{\pi}) - J(\boldsymbol{\mu}) > 0$. \square

B Additional Related Works

Task Planning with LLMs. LLMs (Chowdhery et al., 2023; OpenAI, 2023; Touvron et al., 2023a,b) trained on a large-scale corpus exhibits notable reasoning abilities via in-context learning (Dong et al., 2022; Abernethy et al., 2023; Akyürek et al., 2023). However, LLMs can also give infeasible plans for embodied agents due to the lack of real-world knowledge. A line of research modifies the open-loop planning framework to a closed-loop one via self-evaluation and reflection. For example, ReAct (Yao et al., 2023b), Reflexion (Shinn et al., 2023), and BeamSearch (Xie et al., 2023b) incorporate the feedback of an LLM evaluator in the prompts after the previous plan is completed. Other works integrate domain knowledge of embodied agents in feedback. For example, RoCo (Mandi et al., 2023) and Inner Monologue (Huang et al., 2022b) design physical verification such as collision checking, object recognition, and scene description for feedback. DoReMi (Guo et al., 2023) leverages LLM to generate physical constraints, and ViLA (Hu et al., 2023b) adopts Vision-Language Model (VLM) as a constraint detector for verification. Another line of research develops advanced reasoning frameworks, including chain-of-thought (Wei et al., 2022; Mu et al., 2023) and tree-of-thought (Yao et al., 2023a). Works like (Zhao et al., 2023; Hao et al., 2023) consider LLMs as a world model (Lin et al., 2023c) and adopt tree search in planning (Hu et al., 2023a). Other works adopt the planning domain definition language (PDDL) for searching in long-horizon problems (Silver et al., 2023; Liu et al., 2023a; Zhou et al., 2023). Our work lies in closed-loop frameworks but has a novel advantage function in feedback, which is different from self-reflection or physical feedback and does not rely on advanced searching algorithms.

Other LLM-based Embodied Agent. Beyond task planning, LLMs also shoulder other roles for embodied agents. (i) **Foundation Policy.** Robot Transformer (Brohan et al., 2023b,a), PaLM-E (Driess et al., 2023), Open-X (Collaboration, 2023), and RoboFlamingo (Li et al., 2023b) use pre-trained LLM or VLM as the foundation policies and fine-tune the parameters with embodied data from real-world tasks. The LLM tokens and action tokens of agents are unified in fine-tuning. (ii) **Code Generator.** Given high-level task descriptions, LLMs can generate executable code by calling the basic control primitives (Liang et al., 2023; Vemprala et al., 2023) or low-level actions (Wang et al., 2023b) of embodied agents. VoxPoser (Huang et al., 2023) leverages the code-writing capabilities of LLMs to compose 3D value maps via VLM and adopt model-predictive control (MPC) for planning. (iii) **Reward Designer.** Text2Reward (Xie et al., 2023a), Language2Reward (Yu et al., 2023), and Eureka (Ma et al., 2023) leverage GPT-4 to produce interpretable reward codes, and allow iterative refinement with feedback. (iv) **Data Generator.** To enhance task-level generalization, GenSim (Wang et al., 2023a) adopts LLMs to propose task curriculum and novel sub-tasks to solve complex tasks. RoboGen (Wang et al., 2023c) proposes a closed-loop process to generate robot data, including proposing tasks, generating simulation environments, decomposing sub-tasks, and solving sub-tasks via RL or MPC.

C Algorithmic Description

In this section, we give the algorithm descriptions of critic regression via Monte Carlo estimation, as well as the process of *ReAd-S* and *ReAd-J* algorithms. We highlight the difference between *ReAd-S* and *ReAd-J* by different colors.

Algorithm 1 Critic regression on \mathcal{D} following $\mu = \pi_{\text{llm}}$

Require: data buffer \mathcal{D} , batch size B , critic Q_θ , the set of agents \mathcal{N}
for iteration $k = 1, \dots, M$ **do**
 for all ordered subsets $\{i_1, i_2, \dots, i_u\} \subseteq \mathcal{N}$ **do**
 compute Monte Carlo return estimates $\mathcal{R}_{s, \mathbf{a}^{i_1:u}}$

$$\mathcal{R}_{s, \mathbf{a}^{i_1:u}} = \sum_{\mathbf{a}^{-i_1:u} \in \mathcal{D}} \sum_{t=0}^T \gamma^t r_t$$

update estimated critic $Q_\theta^{i_1:u}$ by using

$$\arg \min_{Q_\mu^{i_1:u}} \mathbb{E}_{s, \mathbf{a}^{i_1:u} \sim \mathcal{D}} \left[\left\| \mathcal{R}_{s, \mathbf{a}^{i_1:u}} - Q_\mu^{i_1:u} \right\|^2 \right]$$

end for
end for

Algorithm 2 *ReAd-S*: Reinforced Advantage Feedback with Sequential Individual Plan Refinement

Require: agent name u^1, \dots, u^N , task horizon T , refinement threshold α , history buffer H , critic Q_θ

Denotation: dialog d ; agent u^i 's plan a^i

initialize timestep $t \leftarrow 0$

initialize observation $s_0 \leftarrow \text{env.reset}()$

while $t < T$ **do**

 initialize joint action $\mathbf{a}_t = \{\}$ and history $H = \{\}$

 set $\alpha \leftarrow 2\alpha$

for $i = 1, \dots, N$ **do**

 initialize the history of evaluated action-score pairs $\mathcal{P} = \{\}$

repeat

$d, a_t^i \leftarrow \text{LLMPrompt}(H, s_t, u_t^i, \mathcal{P})$

$\mathbb{S}_{\text{ReAd-S}}(a_t^i) = Q_\theta^{1:i}(s_t, \mathbf{a}_t^{1:i-1}, a_t^i) - Q_\theta^{1:i-1}(s_t, \mathbf{a}_t^{1:i-1})$

$\mathcal{P} \leftarrow \mathcal{P} \cup \{(s_t, \mathbf{a}_t^{1:i-1}, a_t^i, \mathbb{S}_{\text{ReAd-S}}(a_t^i))\}$

$\alpha \leftarrow \alpha/2$

until $\mathbb{S}_{\text{ReAd-S}}(a_t^i) > \alpha$

$H \leftarrow H \cup \{d\}$

end for

$\sigma_t \leftarrow \text{MotionPlanner}(o_t, \mathbf{a}_t)$

$o_{t+1}, \text{done} \leftarrow \text{env.step}(\sigma_t)$

if done is *True* **then**

break

end if

end while

Algorithm 3 *ReAd-J*: Reinforced Advantage Feedback with Joint Plan Refinement

Require: agent name u^1, \dots, u^N , task horizon T , pick action threshold α , history buffer H , critic Q_θ , discount factor γ

Denotation: dialog d ; Joint WAIT action w

set $H = \{\}$

initialize timestep $t \leftarrow 0$

initialize observation $s_0 \leftarrow \text{env.reset}()$

while $t < T$ **do**

 set $\alpha \leftarrow 2\alpha$

 initialize the history of evaluated action-score pairs $\mathcal{P} = \{\}$

repeat

$d, \mathbf{a}_t \leftarrow \text{LLMPrompt}(H, s_t, [u^1, \dots, u^N], \mathcal{P})$

$\mathbb{S}_{\text{ReAd-J}}(\mathbf{a}_t) = Q_\theta(s_t, \mathbf{a}_t) - \frac{1}{\gamma} Q_\theta(s_t, w)$

$\mathcal{P} \leftarrow \mathcal{P} \cup \{(s_t, \mathbf{a}_t, \mathbb{S}_{\text{ReAd-J}}(\mathbf{a}_t))\}$

$\alpha \leftarrow \alpha/2$

until $\mathbb{S}_{\text{ReAd-J}}(\mathbf{a}_t) > \alpha$

$H \leftarrow \{d\}$

$\sigma_t \leftarrow \text{MotionPlanner}(o_t, \mathbf{a}_t)$

$o_{t+1}, \text{done} \leftarrow \text{env.step}(\sigma_t)$

if done is *True* **then**

break

end if

end while

D Environment Details

We use Difficult Variants of RoCoBench (*DV-RoCoBench*) adapted from RoCoBench (Mandi et al., 2023) and *Overcooked-AI* (Carroll et al., 2019) in our experiments. *DV-RoCoBench* involves three tasks: Sweep Floor, Make Sandwich and Sort Cubes. And we choose two representative scenarios – Cramped Room and Forced Coordination from *Overcooked-AI* in our experiments. In this section, we present a comprehensive overview of the task specifications along with the difficulty modifications we have made in *DV-RoCoBench* and the scenario specifications in two scenarios of *Overcooked-AI*.

As for *DV-RoCoBench*, we directly inherit the action set and quantity of robots from RoCoBench, but design diverse task goals to introduce different difficulty levels. In original RoCoBench, the action set is not the same among different tasks.

As for *Overcooked-AI*, different scenarios share the same action space but are initialized with different kitchen layouts.

D.1 Sweep Floor

Task Description. In this task, the two robots are positioned on opposite sides of the table. Each robot arm equipped with a dustpan and broom must collaborate to efficiently sweep all cubes of the designated color into the dustpan. Subsequently, the robot that holds the dustpan is responsible for disposing of the collected cubes in the trash bin. In this environment, two distinct types of robots with different action sets are used.

1. UR5E robot holding a dustpan (‘Alice’): can move to all cubes and can perform only three operations: MOVE, DUMP, and WAIT.
2. Franka Panda holding a broom (‘Bob’): can move to all cubes and can perform only three operations: MOVE, SWEEP, and WAIT.
3. Action sets: (i) MOVE [target]: target can only be a cube. (ii) DUMP: pour all cubes in the dustpan into the trash bin. (iii) SWEEP [target]: sweep the target cube into the dustpan. (iv) WAIT.

Difficulty Settings. We shift the task goal from sweeping away all the cubes to sweeping away the cubes of a given color. We establish 5 distinct difficulty levels based on the number of cubes and the number of the target cubes. By increasing the difficulty level step by step, the quantity of all cubes and the cubes of a given color increase also gradually, as shown in Figure 4.

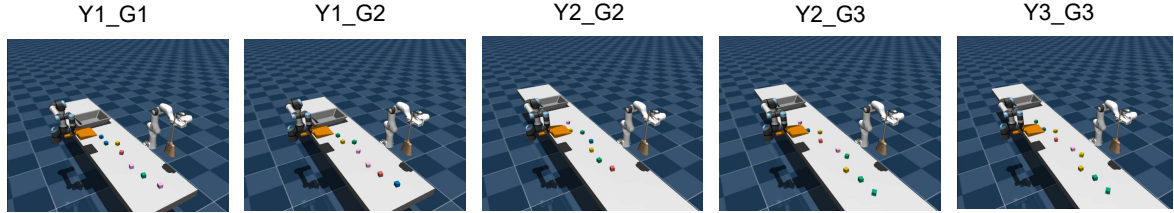


Figure 4: The initial states of the 5 difficulty levels in modified Sweep Floor. The yellow and green squares are the ones to be swept in this task. The first three tasks have a total of 7 squares, while the last two have 9. We assess task difficulty based on the number of cubes to be swept and the total cube number. For example, the Y1_G1 in the figure represents 1 yellow cube and 1 green cube needs to be swept.

D.2 Make Sandwich

Task Description. In this task, two robots are positioned on opposite sides of a table to assemble a sandwich based on a given recipe, requiring collaborative effort to collect and stack the ingredients in the specified order until all components have been properly arranged. This environment accommodates two distinct types of robots capable of executing all actions in the action set. Each robot has a restricted range to manipulate the cubes.

1. UR5E robot ('Chad'): can only retrieve the food on the right side.
2. Humanoid robot ('Dave'): can only retrieve the food on the left side.
3. Action set: 1) PICK [object]: object must be a food. 2) PUT [object] on [target]: object must be a food and target could be a food, cutting_board, or table. 3) WAIT.

Difficulty Settings. We establish 4 distinct difficulty levels dependent on the length of the recipe. A longer recipe requires more complex collaboration between humanoid and robot arm. The recipe lengths for these different settings are set to 3, 5, 7, and 9, respectively, as shown in Figure 5.

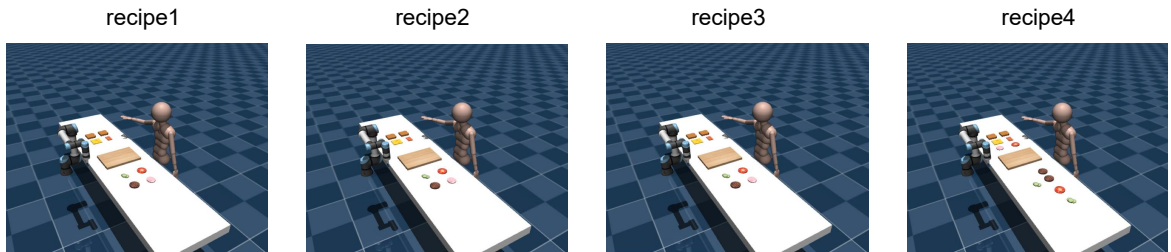


Figure 5: The initial states of the 4 difficulty levels in modified Make Sandwich. The initial three tasks shared the same food and layout, differing only in the length of the recipe. Conversely, the final task presented distinct food and layout, accompanied by a lengthier recipe. The recipe lengths for four tasks are set to 3, 5, 7, and 9, respectively.

D.3 Sort Cubes

Task Description. The task requires three robots positioned on opposite sides of a table to collaboratively place three target blocks in specific locations, utilizing their limited range of motion and assisting each

other as needed. The current environment consists of three robots capable of executing all actions in the action set, albeit with limited mobility range.

1. UR5E with robotic gripper ('Alice'): must put the blue square on panel2, can only reach: panel1, panel2, panel3.
2. Franka Panda ('Bob'): must put pink polygon on panel4, can only reach: panel3, panel4, panel5.
3. UR5E with suction gripper ('Chad'): must put yellow trapezoid on panel6, can only reach: panel5, panel6, panel7.
4. Action set: 1) PICK [object] PLACE [panelX]: the object must be a cube and panelX cannot be the target panel of another cube. 2) WAIT.

Difficulty Settings. We establish 5 difficulty levels based on the distance of the three blocks towards their corresponding target location. Since each robot has limited range of motion, picking further cube to the target location requires more complex collaboration between three robot arms.

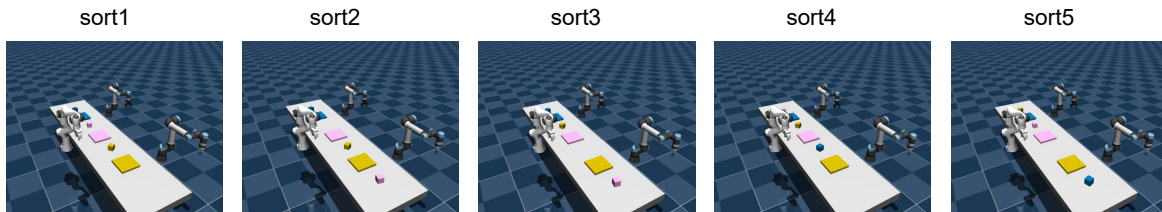


Figure 6: The initial states of the 5 difficulty levels in modified Sort Cubes. In these tasks, we orchestrated the initial placement of each block, and gauged difficulty based on the cumulative distance between the three blocks and the target panel. The shape of the three cubes was modified to avoid the robot's inability to pick up the objects due to their shape.

D.4 Overcooked-AI

Overcooked-AI (Carroll et al., 2019) is a fully cooperative multi-agent benchmark environment based on the wildly popular video game *Overcooked*. In this environment, agents need to deliver soups as fast as possible. Each soup requires placing up to 3 ingredients in a pot, waiting for the soup to cook, and having an agent pick up the soup and deliver it. In details, two agents are originally required to make as much soup as possible in limited timesteps with high coordination efficiency. Agents place a specified number of onions in a pot, leave them to cook for a specified number of timesteps, put the resulting soup in a dish, and serve it, giving all agents a reward. The capacity of all agents to pick up items is 1. Every agent can only carry 1 item such as the dish and the onion.

The environment consists of 5 different kitchen scenarios, covering from low-level motion coordination challenges to high-level strategy coordination challenges. In our experiment, we chose two representative scenarios: **Cramped Room** and **Forced Coordination**, and set the number of ingredients to make soups as 2 and the timesteps to cook as 2. Importantly, to enable measuring with the success rate metric, we modify the task as cooking and delivering a soup to the service counter within a specified number of timesteps.

The action set of this environment is as follows:

1. north: agent moves one step north. If agent collides with another object, it will not move.
2. south: agent moves one step south. Same as the previous term.
3. east: agent moves one step east. Same as the previous term.
4. west: agent moves one step west. Same as the previous term.

5. interact: agent interacts with a object, including picking up or putting down an item, turning on the cooking table, and putting the cooked soup in the dish.
6. stay: agent does nothing.

The first four actions (north, south, east, and west) cover the movement of the agent, and the interact action enables the interaction between the agent and other objects. We use Figure 7 to explain the above rules:

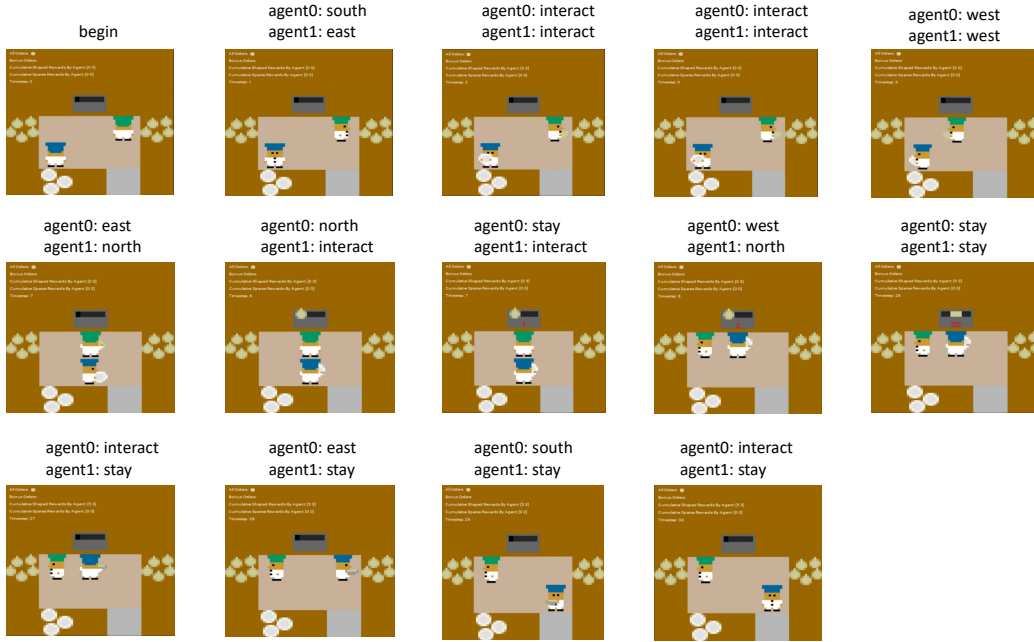


Figure 7: In 2nd frame, since both agents collide with the workbench, the agents merely change their current orientation. In 4th frame, since both agents have picked up an object in their hands, executing "interact" again will not pick up additional items. In 7th frame, agent1 places the onion on the cooking table. And in 8th frame, agent1 turns on the cooking table and starts cooking. In 10th and 11th frames, the soup is done and then put in a dish by agent0. In the last frame, agent0 serves the cooked soup.

Cramped Room. Two agents collaborate in a relatively small kitchen, and thus two agents must be extremely careful to avoid collisions in order to complete the cooking task as quickly as possible. The scenario is shown in the Figure 7.

Forced Coordination. The working spaces of two agents are completely separated, where one agent only has access to the cooking table and the service counter and the other only has access to onions and dishes. The scenario is shown in the Figure 8.

E Additional Experimental Results

In this section, we give the detailed experiment results of 3 tasks in *DV-RoCoBench* and 2 scenarios in *Overcooked-AI*. We also show the execution screenshots of our method and baselines in the representative environments.



Figure 8: In this task, agent0 must wait for agent1 to deliver the onion to the table before agent0 can place it on the cooking table, and after the soup is ready, agent0 must wait for agent1 to place the plate on the table before it can serve the soup and deliver it to the service table.

E.1 Comparison among Chosen Algorithms

Table 3: Overview of the key properties that distinguish four methods. (i) **State Type**: whether the environment state included in the prompt is global or not; (ii) **Planning Scheme**: whether LLM output plans sequentially or not; (iii) **History Info**: whether all the history before is reserved in the prompt or not.

	STATE TYPE	PLANNING SCHEME	HISTORY INFO	FEEDBACK TYPE
RoCo	PARTIAL	SEQUENTIAL	ALL PREVIOUS ROUNDS	PHYSICAL VERIFICATION
READ-S	PARTIAL	SEQUENTIAL	LAST ROUND	ADVANTAGE SCORE
CENTRAL-PLAN	GLOBAL	PARALLEL	ALL PREVIOUS ROUNDS	PHYSICAL VERIFICATION
READ-J	GLOBAL	PARALLEL	LAST ROUND	ADVANTAGE SCORE
REACT	GLOBAL	PARALLEL	ALL PREVIOUS ROUNDS	PHYSICAL VERIFICATION
REFLEXION	GLOBAL	PARALLEL	ALL PREVIOUS ROUNDS	PHYSICAL VERIFICATION
MINDAGENT	GLOBAL	PARALLEL	ALL PREVIOUS ROUNDS	PHYSICAL VERIFICATION

E.2 Additional Experiments on adapted Overcooked-AI

We impose the maximum number of environment steps per episode to 20 in Cramped Room, and 25 in Forced Coordination. Specifically, for our adapted **Cramped Room** and **Forced Coordination**, we deliberately set the maximum environment steps almost equal to the least number of environment steps for accomplishing the task, thereby presenting a challenge for highly effective coordination.

Due to the expensive cost of sequential planning with more environment steps in *Overcooked-AI*, we only evaluate the performance of methods that generate joint plans in a parallel manner. Figure 9 illustrates the results on the adapted *Overcooked-AI*. As shown in Figure 9, our methods achieve a significantly higher SR compared with the methods relying on *physical verification* as feedback in *Overcooked-AI*. Due to the heavy coordination challenges inherent to *Overcooked-AI*, LLM-based agents cannot advance toward task completion unless the LLM planner generates highly collaborative plans.

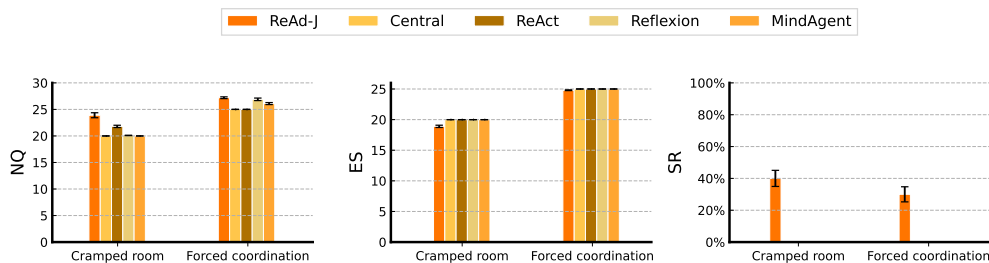


Figure 9: We report mean SR (\uparrow), ES (\downarrow), and NQ (\downarrow) in two scenarios of *Overcooked-AI* averaged over 10 random seeds. The detailed score is given in Table 5 of §E.3.

E.3 Detailed Results on DV-RoCoBench and Overcooked-AI

The results of all experiments are shown in Table 4, and Table 5. SR, NQ and ES represent success rates, the average number of requests to LLMs, and rounds of environment interactions, respectively. We have provided a detailed introduction to these metrics in §5.1.

Table 4: The detailed results of the comparison in different tasks with various difficulty levels in *DV-RoCoBench*. The mean value and standard error are calculated over 10 random seeds.

		RoCo			REACT			CENTRAL PLAN			REFLEXION		
		SR	NQ	ES	SR	NQ	ES	SR	NQ	ES	SR	NQ	ES
SWEEP	Y1_G1	0.9±0.32	14.4±5.95	6.2±3.12	1.0±0.00	5.5±0.50	5.5±0.50	0.4±0.52	15.3±0.48	11.2±4.92	1.0±0.00	5.0±0.00	5.0±0.00
	Y1_G2	1.0±0.00	24.2±4.18	8.9±1.45	1.0±0.00	8.2±0.25	8.2±0.25	1.0±0.00	7.8±1.99	7.8±1.99	1.0±0.00	7.0±0.00	7.0±0.00
	Y2_G2	1.0±0.00	29.1±5.40	10.6±1.35	1.0±0.00	10.0±0.00	10.0±0.00	0.8±0.42	12.7±1.77	12.7±1.77	1.0±0.00	10.1±0.10	10.0±0.00
	Y2_G3	0.7±0.48	36.7±6.63	13.5±1.27	0.6±0.16	14.4±0.67	13.8±0.33	0.2±0.42	14.6±0.97	14.6±0.97	0.7±0.15	14.3±0.87	12.9±0.48
SANDWICH	Y3_G3	0.6±0.52	41.8±7.73	14.7±0.48	0.4±0.16	15.2±0.25	14.9±0.32	0.0±0.00	15.0±0.00	15.0±0.00	0.3±0.15	15.1±0.23	14.9±0.10
	RECIPE1	1.0±0.00	13.2±3.74	4.7±0.67	1.0±0.00	4.0±0.00	4.0±0.00	1.0±0.00	6.2±0.63	4.0±0.00	1.0±0.00	5.0±0.00	4.0±0.00
	RECIPE2	0.9±0.32	28.9±11.25	9.1±2.42	1.0±0.00	6.0±0.00	6.0±0.00	1.0±0.00	8.2±0.42	6.0±0.00	1.0±0.00	6.8±0.13	6.0±0.00
	RECIPE3	0.8±0.42	33.7±10.00	11.5±2.99	0.7±0.15	12.9±2.61	10.1±1.07	1.0±0.00	10.2±0.42	8.0±0.00	0.6±0.16	14.9±2.47	10.8±1.14
SORT	RECIPE4	0.5±0.53	43.1±17.84	13.1±2.47	0.6±0.16	16.7±2.60	12.5±0.75	0.4±0.52	80.5±53.35	14.2±1.14	0.5±0.17	17.7±2.39	13.1±0.67
	SORT1	1.0±0.00	3.3±0.95	1.1±0.32	1.0±0.00	1.2±0.13	1.0±0.00	1.0±0.00	1.0±0.00	1.0±0.00	1.0±0.00	1.2±0.13	1.0±0.00
	SORT2	1.0±0.00	13.5±4.67	3.4±0.52	0.6±0.16	14.8±4.56	7.8±1.96	1.0±0.00	16.9±9.13	2.6±0.52	1.0±0.00	5.5±0.48	2.9±0.10
	SORT3	1.0±0.00	18.6±15.10	4.9±2.60	0.8±0.13	19.4±6.18	6.4±1.45	1.0±0.00	8.3±4.32	2.3±0.95	1.0±0.00	6.6±0.50	4.7±0.33
AVERAGE	SORT4	1.0±0.00	24.8±9.37	6.4±1.78	0.8±0.13	24.0±11.31	6.1±1.49	1.0±0.00	37.2±25.05	7.1±2.77	0.7±0.13	19.2±6.83	7.1±1.45
	SORT5	1.0±0.00	38.5±9.96	7.4±2.95	0.7±0.15	17.3±3.00	8.4±1.59	0.6±0.52	128.4±115.99	11.0±3.97	0.8±0.13	13.9±3.27	6.9±1.43
AVERAGE		0.89±0.19	25.99±8.06	8.25±1.74	0.80±0.09	12.11±2.29	8.19±0.69	0.74±0.17	25.88±15.32	8.39±1.36	0.83±0.06	10.16±1.24	7.59±0.41

		MIND			READ-S			READ-J		
		SR	NQ	ES	SR	NQ	ES	SR	NQ	ES
SWEEP	Y1_G1	1.0±0.00	5.0±0.00	5.0±0.00	1.0±0.00	10.4±0.52	5.0±0.00	1.0±0.00	5.9±0.99	5.0±0.00
	Y1_G2	1.0±0.00	7.1±0.10	7.1±0.10	1.0±0.00	14.4±0.84	7.0±0.00	1.0±0.00	7.6±0.70	7.0±0.00
	Y2_G2	1.0±0.00	9.9±0.18	9.8±0.13	1.0±0.00	19.9±3.28	9.4±0.70	1.0±0.00	13.0±4.32	9.0±0.00
	Y2_G3	0.7±0.15	13.4±0.48	13.4±0.48	0.9±0.32	26.8±5.20	12.2±1.32	1.0±0.00	16.4±6.02	11.7±1.49
SANDWICH	Y3_G3	0.2±0.13	15.1±0.10	15.0±0.00	0.8±0.42	31.4±3.50	14.0±0.82	0.8±0.42	16.4±1.71	13.4±0.84
	RECIPE1	1.0±0.00	5.1±0.10	4.0±0.00	1.0±0.00	10.5±4.74	4.2±0.42	1.0±0.00	4.3±0.48	4.0±0.00
	RECIPE2	1.0±0.00	6.6±0.16	6.0±0.00	1.0±0.00	14.5±2.46	6.4±0.52	1.0±0.00	6.5±0.85	6.0±0.00
	RECIPE3	0.7±0.16	12.4±1.92	10.1±1.07	1.0±0.00	22.1±5.22	8.9±0.88	1.0±0.00	14.6±8.04	8.9±1.00
SORT	RECIPE4	0.6±0.16	16.5±2.24	12.7±0.72	1.0±0.00	27.9±8.06	11.1±1.73	1.0±0.00	10.8±0.42	10.0±0.00
	SORT1	1.0±0.00	1.2±0.13	1.0±0.00	1.0±0.00	3.4±0.52	1.0±0.00	1.0±0.00	1.1±0.32	1.1±0.32
	SORT2	1.0±0.00	6.1±1.12	3.2±0.33	1.0±0.00	10.8±2.53	3.1±0.32	1.0±0.00	7.3±2.91	3.3±0.48
	SORT3	0.8±0.13	11.1±3.70	6.2±1.54	1.0±0.00	17.5±2.80	3.9±0.57	1.0±0.00	8.3±3.80	3.4±0.84
AVERAGE	SORT4	0.9±0.10	22.6±9.62	5.9±1.12	1.0±0.00	21.6±7.07	3.7±0.67	1.0±0.00	18.8±6.29	4.3±0.95
	SORT5	0.8±0.13	18.0±4.12	7.8±1.35	1.0±0.00	33.5±6.35	6.1±0.88	1.0±0.00	17.3±11.87	4.4±1.26
AVERAGE		0.84±0.07	10.72±1.71	7.66±0.49	0.98±0.05	18.91±3.79	6.86±0.63	0.99±0.03	10.59±3.48	6.54±0.51

Table 5: The detailed results of the comparison in two scenarios in *Overcooked-AI*. The mean value and standard error are calculated over 10 random seeds.

		CRAMPED_ROOM			FORCED_COORDINATION			AVERAGE		
		SR	NQ	ES	SR	NQ	ES	SR	NQ	ES
REACT		0.0±0.00	20.1±0.10	20.0±0.00	0.0±0.00	26.9±0.75	25.0±0.00	0.00±0.00	23.50±0.43	22.50±0.00
REFLEXION		0.0±0.00	20.0±0.00	20.0±0.00	0.0±0.00	26.1±0.60	25.0±0.00	0.00±0.00	23.05±0.30	22.50±0.00
MINDAGENT		0.0±0.00	20.8±0.47	20.0±0.00	0.0±0.00	26.9±0.80	25.0±0.00	0.00±0.00	23.85±0.64	22.50±0.00
CENTRAL		0.0±0.00	20.0±0.00	20.0±0.00	0.0±0.00	25.0±0.00	25.0±0.00	0.00±0.00	22.50±0.00	22.50±0.00
READ-J		0.4±0.16	23.9±1.49	18.9±0.59	0.3±0.15	27.2±0.53	24.8±0.20	0.35±0.16	25.55±1.01	21.85±0.40

E.4 Extended Experiment with Llama-3.1-70B-Instruct

Here, we instead use Llama-3.1-70B-Instruct (Dubey et al., 2024) as the basic LLM policy to validate that our algorithm can improve the performance of not only the closed-source models but also the open-source models. We select *Y2_G3* as the task for evaluation, and compare our *ReAd-J* with other baselines including Central Plan, ReAct, Reflexion and MindAgent. The result is reported in Table 6. In terms of the prompt and generation parameters of Llama 3.1-70B in additional experiments, we keep the prompt essentially unchanged. We coarsely search for suitable parameters for the Llama 3.1 70B instruct model. The current generation parameters are determined by a simple grid search on them. Finally, we set the temperature as 0 and top_p as 0.1.

Most methods have a 10%-20% decline in SR, with a slight increase in NQ and ES. Judging from the performance of task *Y2_G3*, GPT-4 has better performance than the Llama-3.1-70B-Instruct. Although using an open-source model like Llama 3.1-70B might result in suboptimal performance, our *ReAd-J* significantly outperforms other baselines based on the same LLM, demonstrating the effectiveness of our method.

Table 6: The detailed result of the comparison in the task *Y2_G3* with Llama-3.1-70B-Instruct as the basic LLM.

	ReAd-J	Central Plan	ReAct	Reflexion	MindAgent
SR	0.9±0.10	0.0±0.00	0.4±0.16	0.5±0.17	0.7±0.15
NQ	13.6±0.56	15.0±0.00	15.0±0.00	13.7±0.37	14.3±0.15
ES	11.8±0.42	15.0±0.00	15.0±0.00	13.6±0.43	14.3±0.15

E.5 Visualization of Robustness Evaluation

We visualize the robustness comparison between *ReAd-S* and *RoCo* for accomplishing *Make Sandwich* recipe3 task when the environment resets at timestep $n = 2$, as shown in Figure 10 and Figure 11.

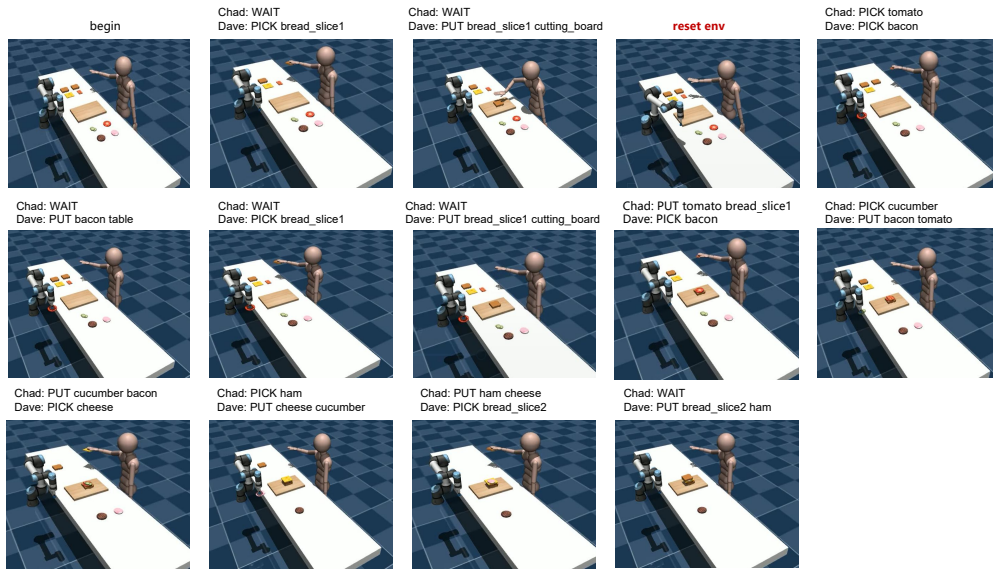


Figure 10: Screenshots of ReAd-S completing the recipe3 task in robustness test. After the environment is reset, our method will be affected by the historical dialogue information in a short period. After being prompted by the advantage function re-evaluated in the new state, our method can make a rapid re-plan based on the new state.

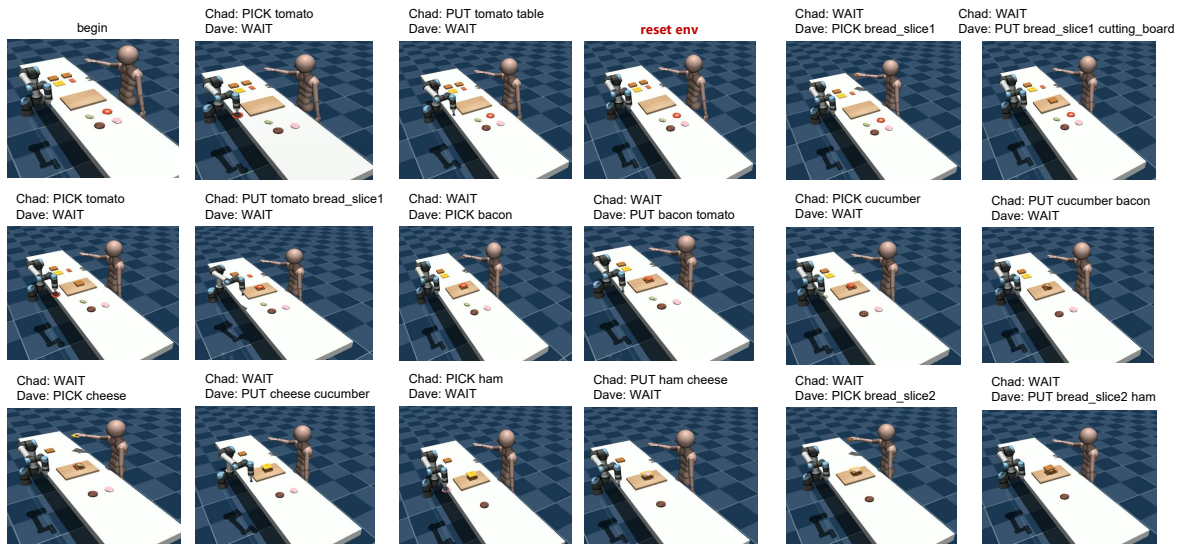


Figure 11: Screenshots of RoCo completing the recipe3 task in robustness test. RoCo needs more steps to recover from the environmental disturbance. Since the reset information is not included in the history, RoCo will be misled by historical information and require multi-round physical feedback to adjust the plan.

E.6 Dataset and Critic Network

Dataset Collection Details. The advantage function relies on the Monte-Carlo estimation of value function with access to an offline dataset collected by π_{llm} . In practice, we employ two techniques to enhance the quality of the collected dataset. (i) We perform data collection using an LLM planner with physical verification, inspired by the RoCo policy (Mandi et al., 2023), which ensures the acquisition of high-quality interaction samples. (ii) Additionally, to address the limited state coverage issue that may arise from directly rolling out the π_{llm} policy, we intentionally reset the environment state to an unreachable state and initiate LLM-planning from that point.

Given that our theoretical analysis demonstrates that our method can achieve a superior policy compared to the behavior policy μ through advantage-weighted regression, it is natural to consider whether a better behavior policy than π_{llm} can be utilized for dataset collection, potentially leading to further policy improvement during optimization. Subsequently, we conduct an ablation study utilizing a mixed dataset collected by an *expert policy* and an *LLM policy*. Our preliminary findings indicate that the inclusion of additional optimal data does not result in performance improvement. We hypothesize that two reasons contribute to these unexpected results. (i) The incorporation of data from a different policy introduces increased variance in Monte-Carlo estimation, thereby reducing the stability of the value functions. Consequently, the value function may produce high-variance outputs, potentially leading to misleading optimization of the LLM planner as prompts. (ii) The LLM planner equipped with enhanced augmentation techniques achieves improved data coverage of the resulting policy. In contrast, the optimal policy is more deterministic, leading to more limited state coverage, which poses challenges for value estimation of out-of-distribution (OOD) states and actions in LLM planning. This issue bears resemblance to the distribution shift problem encountered in offline RL (Levine et al., 2020; Xie et al., 2021).

We describe the differences between *expert policy* and an *LLM policy* in detail here.

- **LLM policy:** This policy is to leverage the reasoning power of LLM to solve specific tasks and use *physical verification* as feedback. It is recommended to use a variant of *ReAd-J* for data collection, which replaces *ReAd* feedback with *physical verification* and uses only the previous round of historical information in the prompts. At each time step t , environment state s_t , robot optional actions, and task goals are added into the prompt in the form of text. And then the LLM takes the prompt as input, generates the joint action \mathbf{a}_t of all robots and get a reward r_t . We store every transition as a tuple (s_t, \mathbf{a}_t, r_t) until the task is accomplished.
- **Expert policy:** Here we implement this policy with human control. This requires a human player to analyze the task and infer the optimal action at each time step. The collected data format is the same as the method described above.

Table 7: An ablation study of data ratio of optimal data and LLM planner data in the offline dataset. The mixing ratio is represented by $X\% : Y\%$, where $X\%$ denotes the percent of samples collected by the *LLM policy*, and $Y\%$ denotes the percent of samples collected by the *optimal policy*.

	NQ	ES	SR
READ-J(0%:100%)	16.4±0.54	13.4±0.27	0.8±0.13
READ-J(50%:50%)	15.8±1.12	13.9±0.35	0.6±0.16
READ-J(100%:0%)	17.6±1.89	13.9±0.41	0.7±0.15
READ-S(0%:100%)	31.4±1.11	14.0±0.26	0.8±0.13
READ-S(50%:50%)	29.1±0.91	13.9±0.31	0.7±0.15
READ-S(100%:0%)	34.2±2.18	14.3±0.30	0.5±0.17

Critic Architecture. The critic learns to estimate the value function of state-action pairs from the dataset. The state includes the environment state and the agent state, where the environment state contains variables of the simulator and the agent state is described by language. The action is also described by language. We adopt the pre-trained BERT Transformer model to extract language features of the agent state and actions. Then we concatenate the output feature with environment state features to some MLP layers to predict the Q -value. The structure of the critic network is given in Figure 12, and the hyper-parameters are given in Table 8.

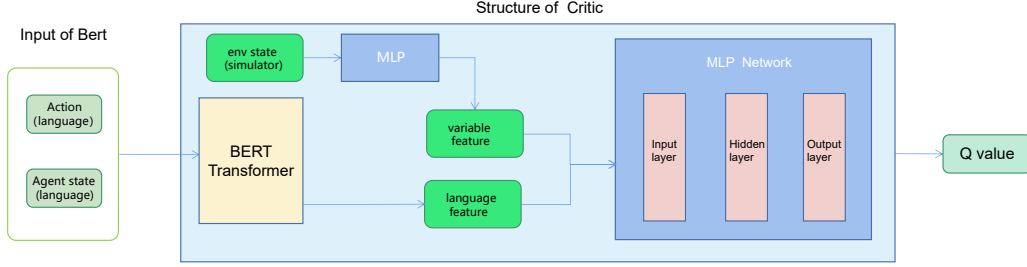


Figure 12: In this figure, the parameters of BERT Transformer are fixed and will not be updated during the training of Critic.

Table 8: The input dimensions for Critic of ReAd-J and ReAd-S are represented by JIS and SIS respectively, while HS represents the hidden layer input dimension, HN represents the number of hidden layers, LR is the learning rate, BS is batch size, TN represents the number of training iterations, SS is the dimension of environment state, and n is the number of robots in the environment.

	JIS	SIS	HS	HN	LR	BS	TN
VALUE	$768+SS$	$n \times 768+SS$	256	1	10^{-3}	32	9×10^5

Token Consumption. We report the details of token consumption on both benchmarks in Table 9 and Table 10 respectively. The total number of tokens consumed includes tokens consumed during pre-sampling data for training critic network. We utilize *LLM policy* to collect data for critic training in the experiment of *DV-RoCoBench*, while the data is collected by *expert policy* in the experiment of *Overcooked-AI*. Obviously, during the phase of planning, *ReAd-S* and *ReAd-J* consume less tokens than all other baselines. In terms of total consumed tokens, *ReAd-J* is comparable to the baselines which also generate joint plans in a parallel manner, and *ReAd-S* is significantly superior to RoCo.

Critic Training. The quantity of trajectories required for critic training depends on how challenging the task is. For 5 difficulty levels in *Sweep Floor*, critic training demands about 70, 120, 240, 600, and 1400 trajectories respectively. For 4 difficulty levels in *Make Sandwich*, about 60 trajectories are needed for critic training. For 5 difficulty levels in *Sort Cube*, critic training demands about 230, 240, 300, 400 and 510 trajectories respectively. For *Cramped room* and *Forced coordination*, the number is about 128 and 2048 respectively. It is important to note that the volume of data utilized for critic training can be adjusted flexibly to align with the specific demands and challenges of the actual situation.

Table 9: Tokens consumed by all methods during the evaluation in *DV-RoCoBench*.

Methods	ReAd-S	ReAd-J	RoCo	Central Plan	ReAct	Reflexion	MindAgent
Tokens for planning	9M	6M	24M	15M	11M	11M	13M
Tokens for training \hat{Q}	7M	7M	-	-	-	-	-
Total tokens	16M	13M	24M	15M	11M	11M	13M

Table 10: Tokens consumed by all methods during the evaluation in *Overcooked-AI*.

Methods	ReAd-J	Central Plan	ReAct	Reflexion	MindAgent
Tokens for planning	1M	2M	4M	3M	4M
Tokens for training \hat{Q}	-	-	-	-	-
Total tokens	1M	2M	4M	3M	4M

F Extended Discussion about Symbol Grounding

In this section, we would like to discuss the LLM grounding problem in embodied tasks beyond our algorithm. Currently, most of available embodied multi-agent collaboration benchmarks (e.g., *DV-RoCoBench* and *Overcooked-AI*) establish the base for LLM grounding by transforming the state/image in the environment to the textual description. Since the LLM is not capable of perceiving the current situation in the environment via visual signals, such a transformation may be achieved by directly using specific object identifiers without visual grounding. However, it may seem to ruin the purpose of LLM grounding where the main role of language is originally to provide a vehicle for establishing common ground and resolving ambiguities. It makes the evaluation of ours and other LLM-based embodied algorithms (Ahn et al., 2022; Yao et al., 2023b; Shinn et al., 2023; Gong et al., 2023) on these benchmarks possibly overestimated on solving the symbol grounding problem (Harnad, 1990).

We acknowledge that directly using fictional object identifiers without visual grounding is a limitation while at the same time it implies that a potential solution to overcome this limitation is to use strong Visual Language Models (VLMs), e.g., GPT-4o. Specifically, it requires identifying the object types (in **Make Sandwich**) or positions (in **Sort Cubes** and **Sweep Floor**), and summarizing the information with a corresponding textual representation, which aligns well with the purpose of symbol grounding. Inspired by this, we conduct a simple but essential experiment to investigate how well GPT-4o captures and describes the necessary information compared with that generated by the object identifiers. Taking the **Forced Coordination** as the test scenario, we give a example in the prompt, which includes a image of current situation of the environment paired with a textual description previously given by the human about this image. Then we ask GPT-4o for generating an appropriate response for the input image, following the template in the example. The example case and test case are shown as Figure 13, and the output textual state and ground truth textual state are listed as follows.

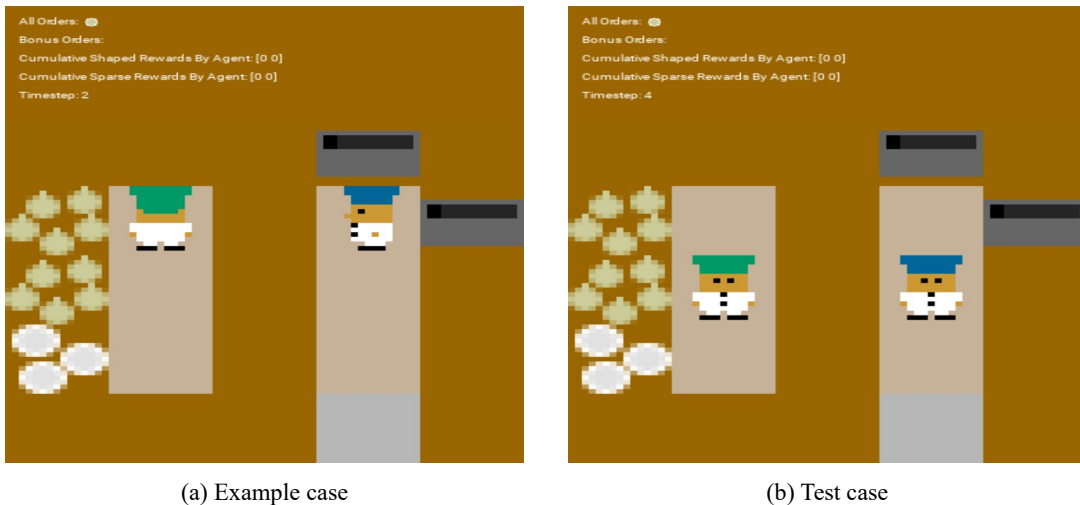


Figure 13: The example case and test case for testing the visual understanding and summarizing capability of GPT-4o.

[Inputting the example image observation]

[Prompt]:

You need to accomplish a task where you need to precisely summarize the necessary information from a given image. We start by introducing the meaning of each character appeared in the *Current Env State* which would be introduced in the example we provide later.

Character Meaning:

The letter X stands for table, P for cooking station, O and o stand for onion, D and d for plates, and S for service desk. When the onion or dish is on the table or being held by agent, an o or d will be added after its corresponding character. When the onion is placed on the cooking table, it will be denoted as p{ø, p{øø means that there are two onions on the cooking table. And when the cooking table cooks the soup, it will show how long it has been cooked, such as p{ø20 means that it has been cooked in 20 time steps. The numbers 1 and 0 represent the agent, and the direction arrow ↑ ↓ ← → represents the direction the agent is facing. Each object occupies a grid size, and the agent moves one grid distance at a time.

Given a image we input, you should first describe the environment status of the image in *Current Env State*, then summarize the events according to *Character Meaning*. Now we provide a specific example. Taking the attached image as input, the standard response corresponding to this image is as follows:

Current Env state:

```
X X X P X
O ↑1 X ←0 P
O   X   X
D   X   X
X X X S X
```

Cook station local (0, 3) (1, 4), there are 0 onions on it, soup has not yet begun to cook

Onions local: (1, 0) (2, 0)

Dishes local: (3, 0)

Server desk local: (4, 3)

Agent0 local: (1, 3), direction: west, hold: nothing

Agent1 local: (1, 1), direction: north, hold: nothing

The above all is the instruction for the task.

[Inputting the test image observation]

[Prompt]:

Please describe this picture following the previous instruction.

[Output]:

Based on the new environment state:

Current Env state:

```
X X X P X
O ↑1 X ↑0 P
O   X   X
D   X   X
X X X S X
```

Cook station local: (0, 3) (1, 4), there are 0 onions on it, soup has not yet begun to cook.

Onions local: (1, 0), (2, 0).

Dishes local: (3, 0).

Server desk local: (4, 3).

Agent0 local: (1, 3), direction: north, hold: nothing.

Agent1 local: (1, 1), direction: north, hold: nothing.

This description follows the format used earlier to capture the environment's status at the current timestep.

[Ground truth]:

Current Env state:

X X X P X

O X P

O ↓1 X ↓0 X

D X X

X X X S X

Cook station local (0, 3) (1, 4), there are 0 onions on it, soup has not yet begun to cook

Onions local: (1, 0) (2, 0)

Dishes local: (3, 0)

Server desk local: (4, 3)

Agent0 local: (2, 3), direction: south, hold: nothing

Agent1 local: (2, 1), direction: south, hold: nothing

Shown in the above response, GPT-4o can generate a textual state with the correct format based on the image and template, but the coordinates and relative positions of objects are inconsistent with the actual situation, which has also been discussed in previous works (Xu et al., 2023). But surprisingly, it can correctly summarize the location and status of all entities in the wrong text-format array. Overall result shows that VLMs are hard to understand spatial relationship from images currently.

G Illustration of the Interaction Process

we illustrate the distinctions between ReAd-S and RoCo by presenting a series of task execution screenshots. In Figure 14 and Figure 15, we compare the screenshots of our method and RoCo algorithm in task *Sweep Floor Y2_G2*. Our method can perform re-plan and correct the initial planning using advantage feedback, which results in a minimum number of environmental interactions. In contrast, RoCo which relies on physical feedback requires more negotiation and interactions with the environment. A similar comparison is shown in Figure 16 and Figure 17 for *Sort Cubes sort4*. A comparison between *ReAd-J* and Central Plan on *Forced Coordination* scenario is shown in Figure 18 and Figure 19.

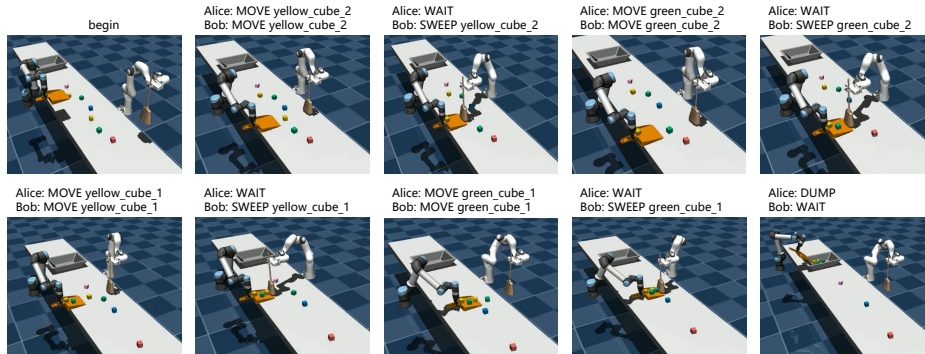


Figure 14: Snapshots of the interaction process of *ReAd-J* in task *Sweep Floor Y2_G2*. Our method obtains the minimum number of environmental interactions needed to complete the task.

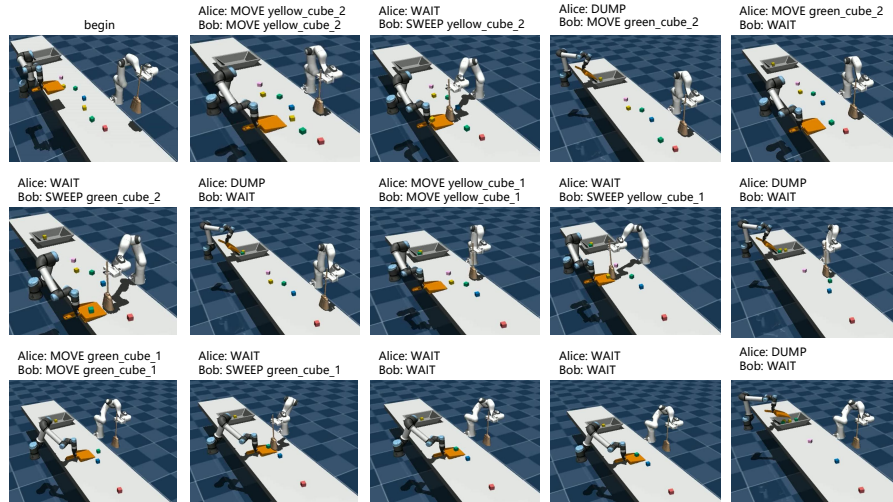


Figure 15: Snapshots of the interaction process of *RoCo* in task *Sweep Floor Y2_G2*. The figure above shows that after planning and sweeping a cube into the dustpan, *RoCo* will dump it into the trash bin. However, after sweeping the last cube into the dustpan, instead of immediately planning to dump it to complete the task, LLM stubbornly believes that the task is done and plans to wait for the next two interactions.

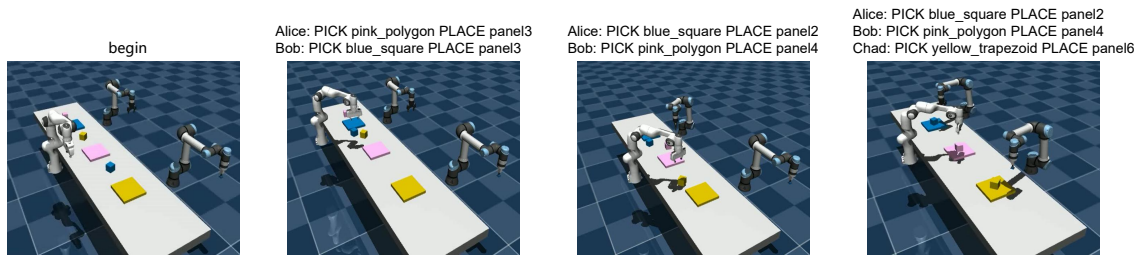


Figure 16: Snapshots of the interaction process of *ReAd-S* in task *Sort Cubes sort4*. This task is challenging and requires the collaboration of three robots and takes a minimum of three steps to complete. Our approach efficiently accomplishes this task with minimal environment interactions.

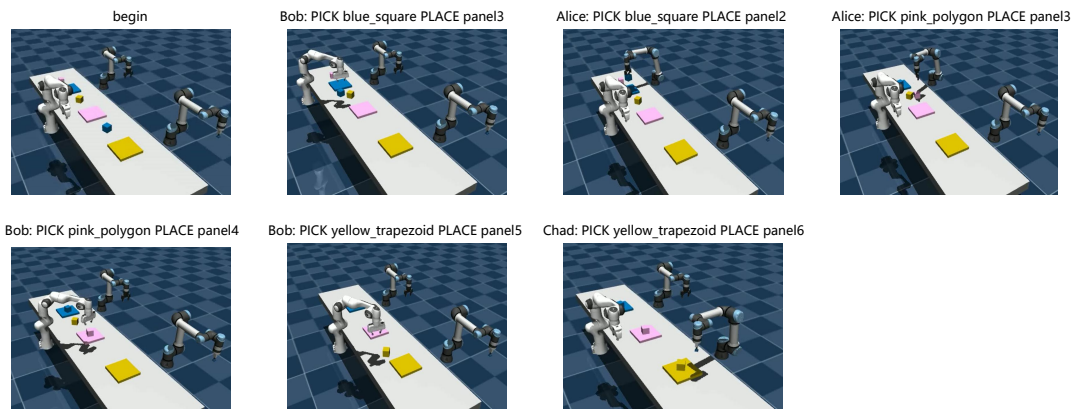


Figure 17: Snapshots of the interaction process of *RoCo* in task *Sort Cubes sort4*. Before the joint actions of all robots are executed, the planning result can only be improved through the dialogue of LLMs. In addition, environmental feedback can be generated only after the agent interacts with the simulator. In contrast, our advantage feedback provides timely feedback in the process of LLM planning for policy improvement before interaction.



Figure 18: Snapshots of the interaction process of *ReAd-J* in task *Forced Coordination*. This task is challenging and requires the collaboration of two agents and takes a minimum of 22 steps to complete. Most of the time, *ReAd-J* can improve the unreasonable planning result generated by LLM, so that *ReAd-J* can complete the task smoothly. However, due to the out-of-distribution (OOD), it is possible to evaluate the advantage value of some unreasonable planning to carry out environmental interaction



Figure 19: Snapshots of the interaction process of *Central Plan* in task *Forced Coordination*. From the screenshot of the interaction process, it can be found that in the *Forced Coordination*, it is difficult for LLM to understand the state of the current environment, so hallucination occurs frequently, resulting in the failure of *Central Plan* to effectively complete the task.

H Examples of Reinforced Advantage Feedback

Format of Advantage Feedback. The Advantage Feedback comprises of [Evaluation Score] and [Improvement Feedback]. If the advantage score of the action is higher than a threshold, the response will only contain [Evaluation Score]. Otherwise, we perform a re-plan to improve the previous action, and the response will include both [Evaluation Score] and [Improvement Feedback].

Below we will briefly show a few examples of the LLM’s planning corrected by advantage feedback, using ReAd-S to complete the Sweep Floor task.

[Alice Response]:
Bob, we have green_cube_1 and green_cube_2 in the dustpan. Let’s MOVE to the trash_bin so I can DUMP these cubes. After that, we can go for any remaining cubes.
PROCEED
NAME Alice ACTION MOVE trash_bin.
[Advantage Feedback]:
[Evaluation Score]:
The advantage score of Alice’s action is -0.6652!
The advantage score is low and the plan need to be changed!
[Improve Feedback]
Alice’s previous response:
Bob, we have green_cube_1 and green_cube_2 in the dustpan. Let’s MOVE to the trash_bin so I can DUMP these cubes. After that, we can go for any remaining cubes.
PROCEED
NAME Alice ACTION MOVE trash_bin
The advantage score is -0.665, it is too low to run. The answer may contain a misunderstanding of the state of the environment, you must change your action to raise the advantage score over 0!
[Alice Response]:
Bob, I made a mistake in my previous plan. Since we already have green_cube_1 and green_cube_2 in the dustpan, I should DUMP them into the trash_bin. I’ll do that while you WAIT.
PROCEED
NAME Alice ACTION DUMP
[Advantage Feedback]:
[Evaluation Score]:
The advantage score of Alice’s action is 17.376!
The advantage score is high enough.

Explain. In this example, the MOVE action can only be used for cubes due to the task setting, and the MOVE of the trash bin is illegal. However, the LLMs learned from the web may consider the MOVE action can also be applied to the trash bin, which does not ground well with the specific task, resulting in the fact of hallucination. Our method can correct this type of error with advantage feedback according to the reward since taking MOVE action to the trash bin will obtain a zero reward and lead to the same next state as the current state.

[Alice Response]:
Bob, we have green_cube_1 and green_cube_2 in the dustpan. Let’s MOVE to the next cube we need to sweep. I suggest we go to pink_cube_1 since it’s the closest cube on the table. Once we’re in position, I will WAIT for you to SWEEP it.
PROCEED
NAME Alice ACTION MOVE pink_cube_1
[Advantage Feedback]:
[Evaluation Score]:
The advantage score of Alice’s action is -0.0927!
The advantage score is low and the plan needs to be changed!
[Improve Feedback]

Alice's previous response:

Bob, we have green_cube_1 and green_cube_2 in the dustpan. Let's MOVE to the next cube we need to sweep. I suggest we go to pink_cube_1 since it's the closest cube on the table. Once we're in position, I will WAIT for you to SWEEP it.

PROCEED

NAME Alice ACTION MOVE pink_cube_1 The advantage score is -0.0927, it is too low to run. The answer may contain a misunderstanding of the state of the environment, you must change your action to raise the advantage score over 0!

[Alice Response]:

Bob, I made a mistake in my previous suggestion. We should not move to pink_cube_1 as it's not one of our targets. Instead, let's DUMP the cubes we have in the dustpan into the trash_bin. I will do that while you WAIT.

PROCEED

NAME Alice ACTION DUMP

[Advantage Feedback]:

[Evaluation Score]:

The advantage score of Alice's action is 18.4184!

The advantage score is high enough.

Explain. In this example, the target colors to sweep are yellow and green. Since the environment also includes many cubes with other colors, LLM may plan to sweep cubes with the wrong colors initially. In such cases, the advantage feedback is helpful to correct the plan generated by the LLM.

[Bob Response]:

Alice, I will WAIT as you move into position for yellow_cube_3.

PROCEED

NAME Bob ACTION WAIT

[Advantage Feedback]:

[Evaluation Score]:

The advantage score of Bob's action is -3.2211!

The score is low and the plan needs to be changed!

[Improve Feedback]

Bob's previous response:

Alice, I will WAIT as you move into position for yellow_cube_3.

PROCEED

NAME Bob ACTION WAIT

The advantage score score is -3.221, it is too low to run, the answer may contain a misunderstanding of the state of the environment, you must change your action to raise the advantage score over -0.2!

[Bob Response]:

Alice, since you are moving to yellow_cube_3, I will also MOVE to yellow_cube_3 to be ready to SWEEP it once you are in position.

PROCEED

NAME Bob ACTION MOVE yellow_cube_3

[Advantage Feedback]:

[Evaluation Score]:

The advantage score of Bob's action is 0.6383!

The advantage score is high enough.

Explain. In this example, the LLM plans for Bob to move to yellow_cube_3 with Alice, it can sweep directly into the dustpan in the next step. However, during the first LLM planning, the LLM plans the WAIT action for Bob. If Bob performs this action at this time, Alice can only wait for Bob to move to yellow_cube_3. Thus, our method performs replanning based on the advantage feedback to reduces the interaction steps to the environment.

I Broader Impact

This paper presents work whose goal is to advance the field of Machine Learning. There are many potential societal consequences of our work, none of which we feel must be specifically highlighted here. This paper presents a novel feedback mechanism which enhances the reasoning and planning capabilities of large language models (LLMs) in multi-agent settings. It has potential implications and societal impacts that are worth considering. First, the overall framework can significantly improve the way robots collaborate on tasks, which could lead to more efficient automation in industries such as manufacturing, logistics, and disaster response. Improved collaboration among robots can lead to increased productivity and reduced human workload. Second, by grounding the reasoning of LLMs in physical tasks, it contributes to the development of AI systems that can make more informed and effective decisions. This advancement can be beneficial across various sectors, including healthcare, where AI could assist in complex diagnostic processes, or in environmental management, where AI could optimize resource allocation. In conclusion, our work presents exciting opportunities for advancing AI and robotics.